CCI
BIOMASS

PRODUCT REGIONAL ASSESSMENT AND INTERCOMPARISON REPORT VERSION 2.0

DOCUMENT REF:	CCI_BIOMASS_PRAIR
DELIVERABLE REF:	D2.1 -PRAIR
VERSION:	2.0
CREATION DATE:	2020-11-30
LAST MODIFIED	2020-12-17

Document Authorship

	NAME	FUNCTION	ORGANISATION	SIGNATURE	DATE
PREPARED	T. Le Toan M. Planells A. Bouvet S. Mermoz	**WP4 Leader**	CESBIO		
PREPARED	R. Lucas	Project Manager	Aberystwyth Uni.		
PREPARED	J. Carreiras	WP4	Sheffield Uni.		
PREPARED	H. Kay	WP9	Aberystwyth Uni.		
VERIFIED	S. Quegan	Science Leader	Sheffield University		
APPROVED					

Document Distribution

ORGANISATION	NAME	QUANTITY
ESA		

Document History

VERSION	DATE	DESCRIPTION	APPROVED
0.1	2020-11-25	First draft version	
1.0	2020-11-25	Version 1.0 accepted	

Document Change Record (from Year 1 to Year 2)

VERSION	DATE	DESCRIPTION	APPROVED
2.0	2019-12-17	First draft of second version	

Document Change Record (From Year 2 to Year 3)

VERSION	DATE	DESCRIPTION	APPROVED
2.0	2020-12-01	First draft of third version	

Table of Contents

Symbols and acronyms ***4***

1 Introduction ***6***

1.1 Purpose and scope **6**

2 Biomes evaluations ***8***

2.1 Wet tropics/subtropics **8**

2.1.1 AGB estimated from airborne Lidar 9

2.1.2 AGB estimated from SLB and CMSKAL airborne Lidar 21

2.1.3 Comparison with AGB map of RDC 25

2.1.4. Data from Ploton et al.,2020 27

2.2 Dry Tropics and Subtropics **30**

2.2.1 Australia 30

2.2.2. Guinea-Bissau 31

2.3 Temperate and Boreal Biomes **35**

2.3.1 Comparison with an existing AGB map (Sweden) 35

2.3.2 Comparison with NEON airborne Lidar data (North America) 36

2.3.3 Temperate forest, Wales 38

Discussions ***42***

Conclusions ***43***

2.4 Mangroves **44**

2.5 Summary on the intercomparison **47**

3 Suggestions of improvements ***49***

3.1 Classification of areas of high AGB **49**

3.2 AGB changes **52**

3. References ***55***

SYMBOLS AND ACRONYMS

ADP	Algorithm Development Plan
AGB	Above-Ground Biomass
ALOS	Advanced Land Observing Satellite
ALS	Airborne Laser Scanning
APBL	Australian Plant Biomass Library
ASAR	Advanced Synthetic Aperture Radar
ATBD	Algorithm Theoretical Basis Document
CCI	Climate Change Initiative
CCI-Biomass	Climate Change Initiative – Biomass
CCI-LC	Climate Change Initiative – Land Cover
CHM	Canopy Height Model
DRC	Democratic Republic of Congo
DUE	Data User Element
E3UB	End to End ECV Uncertainty Budget
EO	Earth Observation
ESA	European Space Agency
F2020	Forests 2020
FBD	Fine Beam Dual
GCOM	Global Change Observation Mission
GEDI	Global Ecosystems Dynamics Investigation
GLAS	Geoscience Laser Altimeter System
GMW	Global Mangrove Watch
HNP	Hitchinbrook Island National Park
ICESAT	Ice, Cloud, and Land Elevation Satellite
JAXA	Japanese Aerospace Exploration Agency
K&C	Kyoto & Carbon
KNP	Kakadu National Park
LiDAR	Light Detection and Ranging
MODIS	Moderate Resolution Imaging Spectroradiometer
NASA	National Aeronautics and Space Adminisration
NCEO	National Centre for Earth Observation
NFI	National Forest Inventory
PALSAR	Phased Array L-band Synthetic Aperture Radar
PSD	Product Specifications Document
PVASR	Product Validation and Algorithm Selection Report

RMSE	Root Mean Square Error
SAR	Synthetic Aperture Radar
SLC	Scan Line Corrector
SMOS	Soil Moisture & Ocean Salinity
SRTM	Shuttle Radar Topography Mission
TC	Total Cover
TERN	Terrestrial Environment Research Network
VCF	Vegetation Continuous Fields
VOD	Vegetation Optical Depth
WCM	Water Cloud Model

Table 1. Applicable documents

ID	TITLE	ISSUE	DATE
RD-1	User Requirements Document		
RD-2	Product Specification Document		
RD-3	Data Access Requirements Document		
RD-4	Algorithm Development Plan		
RD-5	Algorithm Theoretical Basis Document		
RD-6	End to End ECV Uncertainty Budget		
RD-7	Product Validation Plan		
RD-8	Algorithm Theoretical Basis Document of GlobBiomass Project		

1 Introduction

1.1 Purpose and scope

The European Space Agency's (ESA) Climate Change Initiative (CCI) Biomass Project aims to a) generate global estimates of above-ground biomass (AGB; Mg ha^{-1}) for the epochs 2017, 2018 and 2010 and b) quantify AGB change between these. This will be achieved using spatially and temporally consistent Earth Observation (EO) datasets and state-of-the-art models and aligning with other datasets produced through the CCI Program. The requirements [RD-1] are for AGB to be provided wall-to-wall over the entire globe for all major woody biomes, with a spatial resolution between 500 m and 1 km (based on satellite observations of 100-200 m), a relative error of less than 20 % where AGB exceeds 50 Mg ha^{-1}, and a fixed error of 10 Mg ha^{-1} where the AGB is below that limit. This differs from the ESA Data User Element (DUE) GlobBiomass project, where the emphasis was also on a global product, but the requirements were for the relative error in AGB being ≤ 30% and the spatial resolution ≤ 500 m. Hence, in CCI Biomass, greater accuracy is required in biomes supporting lower levels of AGB (e.g., the dry tropics/subtropics and boreal zones).

The scope of this Product Regional Assessment and Intercomparison Report (PRAIR, new designation of the former PVASR) is to assess the global AGB specified in the Product Specifications Document (PSD) [RD-2], and to investigate potential ways to improve the estimation of AGB at a biome level. The algorithms described in the Algorithm Theoretical Basis Document (ATBD) [RD-5] are assessed in terms of their performance globally and for specific biomes (e.g., wet tropics/subtropics) and forest types (e.g., mangroves). An independent

review of the biomass maps is provided by exploiting reference datasets, mainly *in situ* and airborne Lidar but also other AGB maps.

In the first version of the PVASR [D2.1 v1], the CCI Biomass algorithm was based on that developed through the ESA DUE GlobBiomass project [RD-8; Rodríguez-Veiga et al., 2019]. The GlobBiomass algorithm was based on the use of the Water Cloud Model (WCM), and relied on an adaptive approach to estimate the model parameters in space and time, and removed the requirement of *in situ* data for training. The algorithm was used to generate a global map of forest AGB for 2010, based on the EO data available for this epoch, namely ENVISAT Advanced Synthetic Aperture Radar (ASAR), Advanced Land Observing satellite (ALOS) Phased Array Type L-band Synthetic Aperture Radar (PALSAR) data and Landsat data.

In the PVASR v1 [D2.1 v1], a number of generic and biome-specific improvements were proposed based on the analysis and review of the GlobBiomass product. The proposed generic improvements concerned primarily the refinement of the WCM and its use. These included: i) reformulating the WCM to relate the radar backscatter directly to AGB, and ii) making use of available *in situ* and Lidar-derived AGB data and relevant classifications of land cover (e.g., mangroves, inundated forests) to improve parameterisation of the WCM (e.g., terms relating to transmissivity, or maximum AGB). Another generic issue addressed concerned compensation of topographic effects on the L-band backscatter data.

Within the Wet Tropics, the AGB is typically underestimated for forests with AGB > 150-200 Mg ha^{-1}. This has been attributed to saturation of C- and L-band SAR backscattering. In addition, for dense forests, it was found that the increased attenuation with high AGB leads to decreases in L-band backscatter (Mermoz et al., 2015). In both cases, lower AGB retrievals have been found at the higher end of the AGB range. For this high AGB range, the following approaches were investigated in the PVASR-v1:

- The Vegetation Optical Depth (VOD) dataset from SMOS (L-band), which has demonstrated sensitivity to AGB in the range of AGB > 200 Mg ha^{-1}. The L-VOD was considered as a candidate for inter-annual change detection, albeit at 1 km resolution, as SMOS has been acquiring data globally and intra-annually since 2009.
- The combination of height (H, m) at 1 km (from Simard 2011, generated from the ICESAT Geoscience Laser Altimeter System (GLAS)) and tree cover (TC; %) from both Landsat (Hansen et al., 2013) and Proba-V were also shown to have a close correspondence with reference airborne Lidar-derived AGB maps. The TC x H layers could only be generated for 2010 as both ICESAT GLAS and Landsat were in operation

during this period. Proba-V data were acquired from 2013 onwards but the use of the derived canopy cover product as an alternative to the Hansen et al. (2013) product was assessed because of better representation over savanna areas (e.g., in Australia). Global Ecosystem Dynamics Investigation (GEDI) data have recently become available (data acquired from 2018).

- The decreasing trend of L-band backscatter data for dense forests (Mermoz et al., 2015). However, there is a need to identify the pixels (or regions) corresponding to dense forest. This is under investigation using existing information and data (e.g., airborne Lidar data) acquired over a range of tropical forests.

During Year 2 of the project, in WP3000, methods developed in Year 1 were refined by taking into account the assessment of the GlobBiomass AGB map and alternative algorithmic advances documented in the PVASR-v1 and in the Algorithm Development Plan (ADP) [RD-4].

The scope of this report is to assess the recently available CCI AGB products for 2010, 2017 and 2018, namely Products Version 2.

Following this introduction, Section 2 provides the comparisons of CCI+ Biomass products 2010, 2017 and 2018 V2 for major forest biomes (the wet tropics/subtropics, dry tropics/subtropics, temperate, boreal, and mangroves). Section 3 outlines some of the general issues associated with AGB retrieval across these biomes and to suggest ways to improve these issues for Year 3.

Works are undertaken on the approach for AGB changes from the CCI AGB products, and making use of other datasets with consistent time series for the epoch under study (2010-2020).

2 Biomes evaluations

2.1 Wet tropics/subtropics

For the wet tropics and sub-tropics, comparisons were made between the CCI+ Biomass maps 2010, 2017, 2018 v.2 against existing AGB biomass maps for Gabon, French Guiana and the Democratic Republic of Congo (DRC), and Kalimantan. These maps were generated with reference to airborne Lidar and *in situ* data.

2.1.1 AGB estimated from airborne Lidar

AGB was estimated from airborne Lidar–derived AGB maps in Gabon (2015-16; AfriSAR campaign – 4 maps), French Guiana (2009; TropiSAR campaign-2 maps; Labrière et al., 2018) (see Figure 1 for detail), and the DRC (one map from numerous Lidar acquisitions; Xu et al., 2017). These maps of AGB were representative of larger areas and were more spatially representative than forest inventory data alone but were derived by referencing these. For each site, the Lidar-derived maps of AGB were resized to the 100 m resolution of the CCI+ Biomass products and a Fast Fourier Transform was used to correct for image shifts.

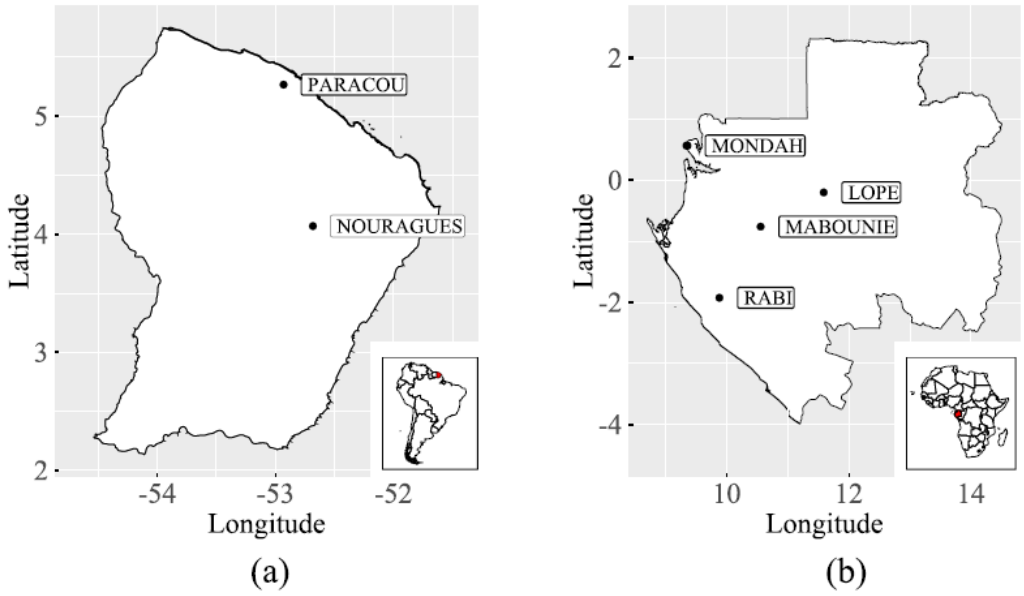

Figure 1: The location of study sites in (a) French Guiana (Nouragues, Paracou) and (b) Gabon (Lopé, Mabounie, Mondah and Rabi).

The relevance and quality of the Lidar derived AGB maps for CCI+ Biomass product comparison need to be considered. Such datasets contain errors and uncertainties from various sources that are well quantified in Labrière et al. (2018). These include those that are inherent to stand biomass estimation (e.g., field-based tree measurement error and uncertainties associated with the allometric equations and sampling error) or associated with the spatial mapping of AGB. Lidar acquisition parameters are also known to influence the quality of AGB mapping. Table 2: Overview of the forest inventory and Lidar datasets acquired during the TropiSAR (2009) and AfriSAR (2015-16) campaigns., extracted from Labrière et al. (2018), indicates the characteristics and dates of forest inventory and the Lidar datasets used for generating locally-derived AGB maps, with these subsequently informing on the quality of the CCI Biomass products.

The height estimation can be biased by the low point density (e.g., when the average point density drops below 4 m^{-2}), which is the case at Lopé and Rabi, and can potentially lead to large errors (up to 125 Mg ha^{-1}) in inferred AGB, especially when the landscape has a

heterogeneous topography. Another source of error in AGB estimation from Lidar is the temporal mismatch between ground and Lidar data acquisitions. The table below shows that for three of the AfriSAR sites (Mabounie, Mondah), the time lag between in situ data and Lidar acquisitions was 5 years (and Rabi, 3 to 5 years). For the other three sites, the time lag was < 1 year. The time lag effect is important where forest disturbances occur, and can be significant for low AGB vegetation (grassland, woody savannah, degraded forest), for which relative change can be significant. However, for many dense forests, mortality and tree recruitment leads to a small change in AGB in 3-5 years.

Table 2: Overview of the forest inventory and Lidar datasets acquired during the TropiSAR (2009) and AfriSAR (2015-16) campaigns.

		Forest inventory dataset				Lidar dataset			
Campaign	Site	Year of forest inventory	Number of permanent plots	Total plot area (ha)	Number of trees with DBH ≥ 10 cm (number of species)	Year of lidar data acquisition	Lidar system and acquisition characteristics (device – carrier – wavelength)	ROI [a] covered by lidar (ha)	Average lidar point density (m^{-2})
TropiSAR (2009)	Nouragues	2010 and 2012	11	34	17350 (823)	2012	RIEGL LMS-Q560 – aircraft – 1.5 µm	2400	19.9 (0.3) [b]
	Paracou (incl. Arbocel)	2009	17	125	79167 (753)	2009	RIEGL LMS-280i – helicopter – 0.9 µm	1100	5.7 (0.1)
AfriSAR (2015–16)	Lopé	2016 [c]	14	12.5	3710 (141)	2015	RIEGL VQ-480i – helicopter – 1.5 µm	5400	2.4 (0.1)
	Mabounié	2012	12	12	4424 (196)	2007	RIEGL LMS-Q560 – aircraft – 1.5 µm	18000	4.3 (0.1)
	Mondah	2016 [c]	19	19	5687 (225)	2011	RIEGL LMS-Q560 – aircraft – 1.5 µm	9800	30.5 (2.3)
	Rabi	2010 to 2012	1	25	11601 (234)	2015	RIEGL VQ-480i – helicopter – 1.5 µm	900	2.5 (0.05)

[a] Note that region of interest (ROI) area might differ from total lidar coverage (e.g. in Mondah where urban areas were also covered but further discarded for the analyses)

[b] Average lidar point density for ground points shown in brackets.

[c] Data from plots set up within the lidar coverage at the study site prior to the main field campaign – data curated by ForestPlots.net – were also included in the analysis.

Gabon -Lopé

Lopé is located near the geographical centre of Gabon (0.20° S, 11.59° E). The hilly landscape (altitude ranging from 200 to 600 m a.s.l.) is dominated by a forest-savannah mosaic, with Aucoumea-dominated and/or Marantaceae forests, where the AGB can exceed 600 Mg ha^{-1}. Savannahs are generally of low AGB (< 100 Mg ha^{-1}) and occur over flatter terrain. Note that the airborne Lidar data were acquired in 2015, and forest inventory data were updated in 2016. The time lags between the Lidar dataset and the 2010, 2017 and 2018 CCI AGB are respectively -5, +2 and +3 years. These differences were more likely to impact on the comparisons over tree savannahs and grasslands compared to dense forest.

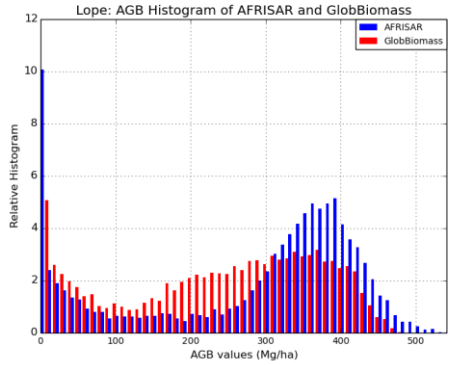
Lope: AGB Histogram of AFRISAR and GlobBiomass
AFRISAR
GlobBiomass
Relative Histogram
AGB values (Mg/ha)

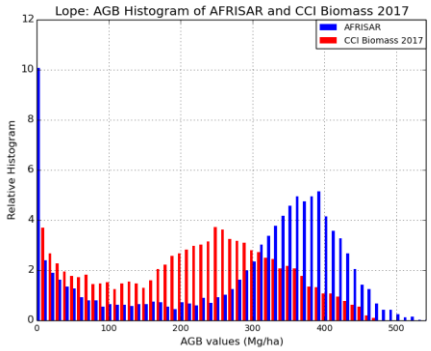
Lope: AGB Histogram of AFRISAR and CCI Biomass 2017
AFRISAR
CCI Biomass 2017
Relative Histogram
AGB values (Mg/ha)

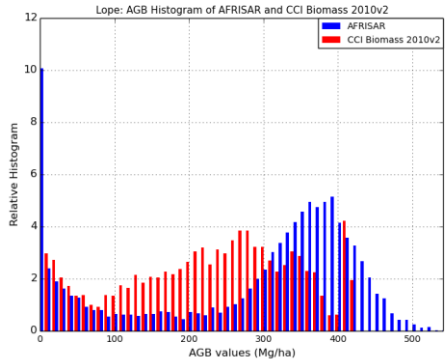
Lope: AGB Histogram of AFRISAR and CCI Biomass 2010v2
AFRISAR
CCI Biomass 2010v2
Relative Histogram
AGB values (Mg/ha)

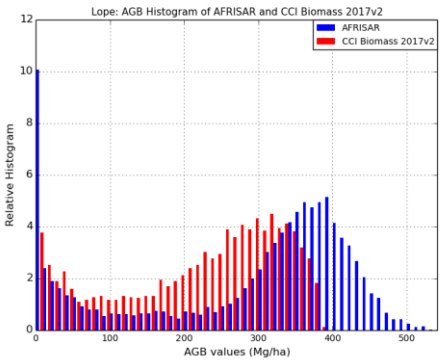
Lope: AGB Histogram of AFRISAR and CCI Biomass 2017v2
AFRISAR
CCI Biomass 2017v2
Relative Histogram
AGB values (Mg/ha)

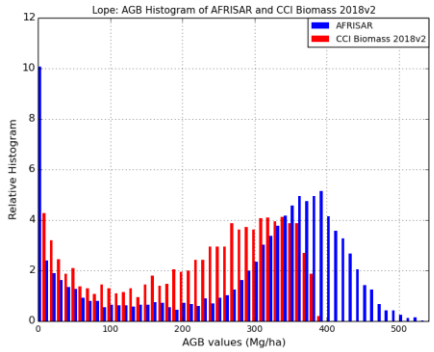
Lope: AGB Histogram of AFRISAR and CCI Biomass 2018v2
AFRISAR
CCI Biomass 2018v2
Relative Histogram
AGB values (Mg/ha)

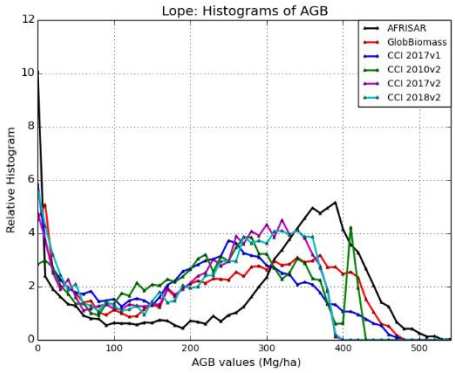
Lope: Histograms of AGB
AFRISAR
GlobBiomass
CCI 2017v1
CCI 2010v2
CCI 2017v2
CCI 2018v2
Relative Histogram
AGB values (Mg/ha)

b

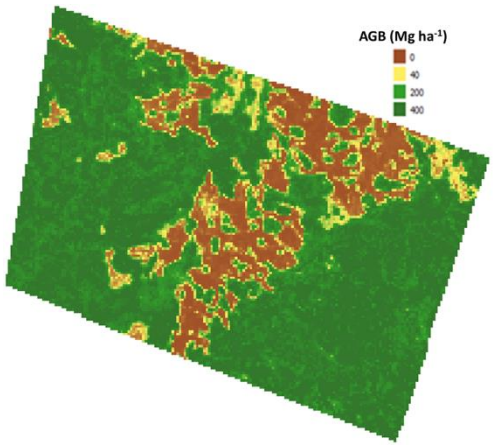

Figure 2: a) Frequency distribution of AGB derived over Lopé, Gabon from airborne Lidar (blue) and from the GlobBiomass 2010 AGB (red, top left) , CCI 2017 AGB v.1 (red, top right), CCI 2010 AGB v.2 (medium left), CCI 2017 AGB v.2 (red, medium right), CCI 2018 AGB v.2 (red, bottom left), and distributions of all the AGB maps (bottom right) .

b) AGB maps derived from AfriSAR Lidar.

The histograms of AGB in the AfriSAR data (Figure 2) show two distributions; the dense forest with an AGB of 250-500 Mg ha^{-1}, with the distribution peak at ~ 380 Mg ha^{-1}, and lower AGB areas (typically < 100 Mg ha^{-1}) associated with savannah (grasslands and sparse woodlands). In the CCI Biomass v2, the peak of the forest distributions is at about 300 Mg ha^{-1}, which is an improvement compared to CCI Biomass v1, which was at 250 Mg ha^{-1}.

For savannah areas (AGB < 100 Mg ha^{-1}), the distributions are overall in good agreement with the LIDAR-derived maps, although there is under-estimation for pixels associated with bare areas (AGB=0). This can partly be attributed to differences in the resolution and acquisition timing of the data used for the generation of the products.

For forest pixels of intermediary range (100 Mg ha^{-}<AGB < 200 Mg ha^{-1}), the CCI Biomass products v2 still overestimate AGB. The drop of the distributions at the high end of AGB 2017 & 2018 v2 at about 380 Mg ha^{-1} indicates a threshold-type artefact.

Gabon -Mabounie

Mabounie is located ca. 180 km Southeast of Libreville (0.76°S, 10.56°E), where the altitude ranges from 25 to 230 m a.s.l. The landscape is mostly forested (of which swamp and temporarily flooded forests constitute a large proportion) but shows evidence of degradation locally. The airborne Lidar data were acquired in 2007, and hence there was a 3, 10 and 11 years difference in the timing with the CCI Biomass maps of 2010, 2017, 2018 respectively. Comparison of the histograms (Figure 3) from the products indicated a better agreement of the distribution between the Lidar map and the 2017 and 2018 v2 products. However, the abrupt end limit of the distribution denotes the use of a maximum threshold in the algorithm, leading to the lack of AGB at the high end (400-450 Mg ha^{-1}), and the difference in the distribution pattern with the Lidar product distribution.

Overall, for Mabounie, there was: a) a noticeable improvement of the v2 products compared to v1, b) small over estimation in the range of 150-250 Mg ha^{-1}, and underestimation of AGB for the dense forest 400-450 Mg ha^{-1}, the latter is probably caused by the use of a maximum threshold in the algorithm.

a)

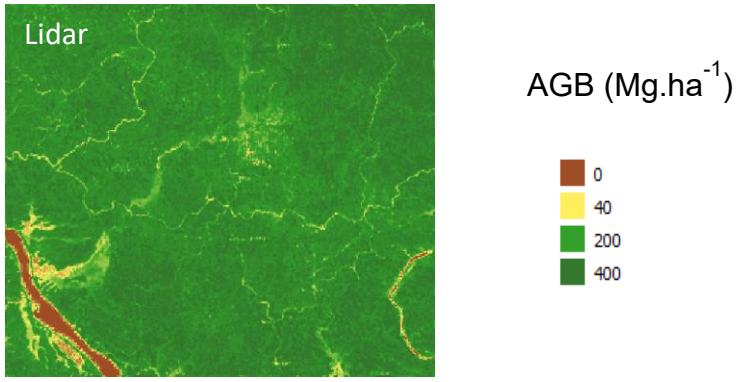

b)

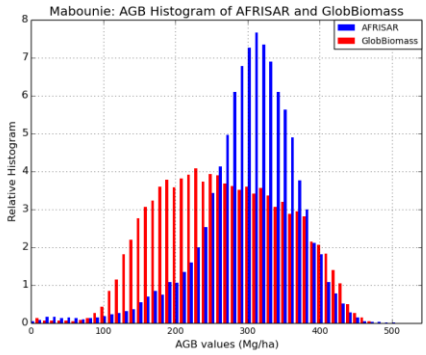

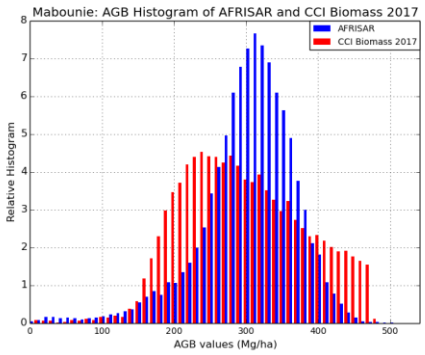

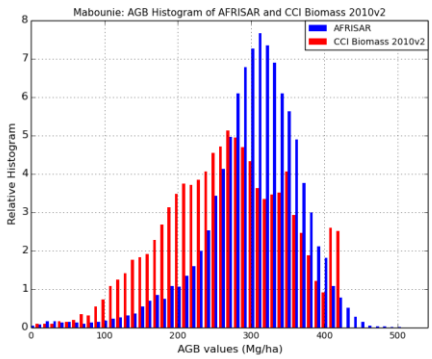

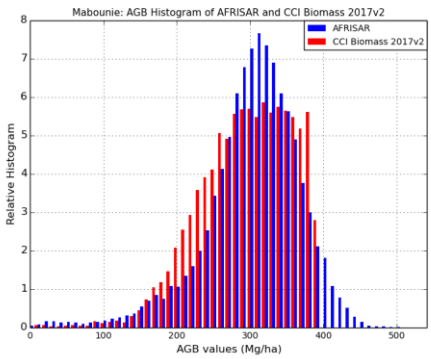

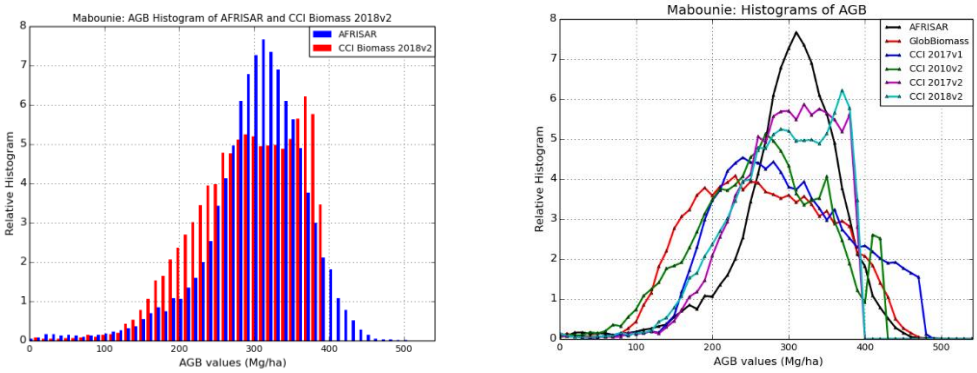

Figure 3: a) AGB maps derived from AfriSAR Lidar (top) b) Frequency distributions of AGB derived over Mabounie, Gabon from airborne Lidar (blue) and from the 2010 GlobBiomass estimated AGB (red, top left), 2017 CCI AGB Year 1 (red, top right), 2010 CCI AGB v2 (red, medium left), 2017 CCI AGB v2 (red, medium right), 2018 CCI AGB v2 (red, bottom right), and from all products (bottom right).

Gabon -Mondah

Mondah is located ca. 25 km northwest of Libreville toward Cap Esterias (0.57°N, 9.35°E) and the altitude seldom exceeds 50 m a.s.l. Different vegetation types occur in this coastal landscape, including Aucoumea-dominated and mixed forests. Whilst significant disturbance occurs, some patches are protected.

Comparison of the AGB estimated from Lidar (acquired in 2011) and the 2010, 2017, 2018 CCI Biomass v2 products (Figure 4) indicated that the histograms of v2 products differ noticeably with the 2017 v1, which showed the best fit with the Lidar map distribution. The histograms of 2017 v2 and 2018 v2 are similar, and quite different from 2010 v2. Forest degradation that occurred after 2010 could explain the bimodal distribution in 2017/2018.
Overall, Mondah presents inconsistencies in the histograms (2017 v1 versus 2017 v2, 2010 v2 versus 2017 v2), but the timing difference between Lidar map and the 2017 CCI map could explain part of the discrepancies.
However, according to Gamma, the cause of discrepancy between 2017 v1 and v2 can be that v1 was based on ALOS-2 data from 2016 and 2017 to increase the density of observations. For v2, only the data of 2017 were used. It is likely that v1 represented a mix of 2016 and 2017 whereas v2 is purely 2017. If there are strong dynamics of the forest, as it is the case in Mondah it is likely these were captured in the maps. On the other hand, the abrupt end at 370 Mg ha^{-1} could be due to an effect of the median filtering applied to 100 forest cover pixels to smoothen some of the stripe effects on the images.

a)

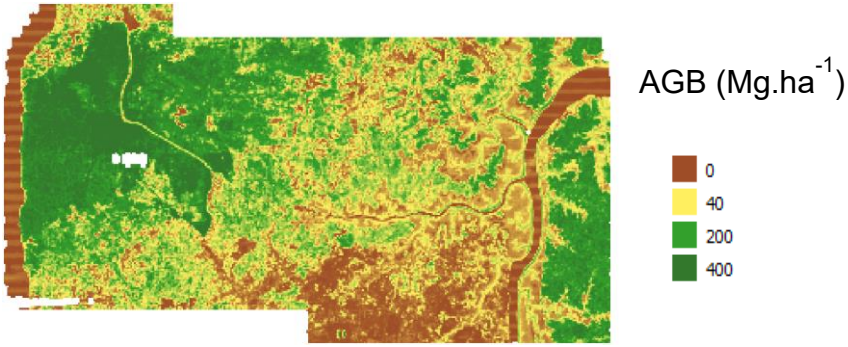
AGB (Mg.ha-1)
0
40
200
400

b)

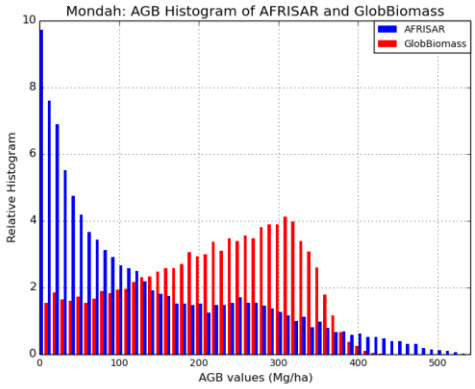
Mondah: AGB Histogram of AFRISAR and GlobBiomass
AFRISAR
GlobBiomass
Relative Histogram
AGB values (Mg/ha)

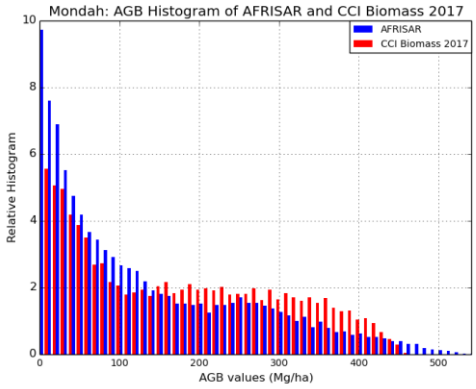
Mondah: AGB Histogram of AFRISAR and CCI Biomass 2017
AFRISAR
CCI Biomass 2017
Relative Histogram
AGB values (Mg/ha)

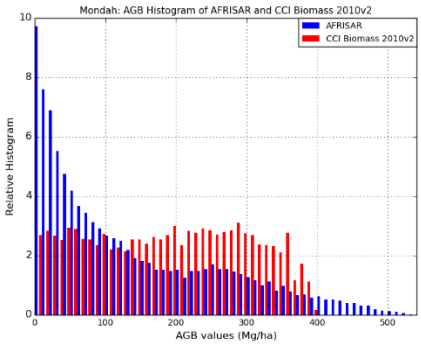
Mondah: AGB Histogram of AFRISAR and CCI Biomass 2010v2
AFRISAR
CCI Biomass 2010v2
Relative Histogram
AGB values (Mg/ha)

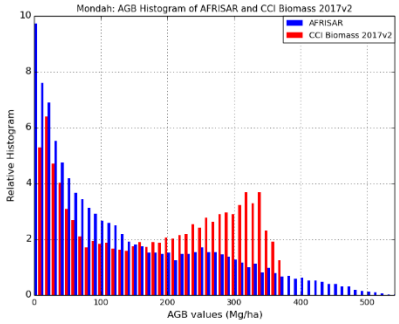
Mondah: AGB Histogram of AFRISAR and CCI Biomass 2017v2
AFRISAR
CCI Biomass 2017v2
Relative Histogram
AGB values (Mg/ha)

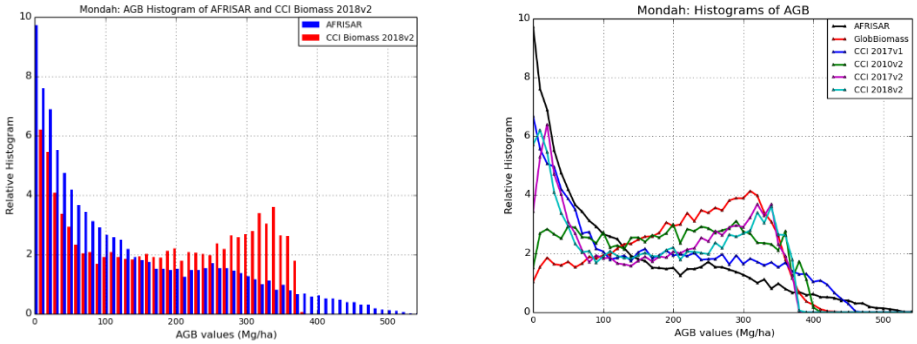

Figure 4: a) AGB maps derived from AfriSAR Lidar (top) b) Frequency distributions of AGB derived over Mondah, Gabon from airborne Lidar (blue) and from the 2010 GlobBiomass estimated AGB (red, top left), 2017 CCI AGB Year 1 (red, top right), 2010 CCI AGB Year 2 (red, medium left), 2017 CCI AGB Year 2 (red, medium right), 2018 CCI AGB Year 2 (red, bottom right), and all the different year's maps (bottom right).

Gabon - Rabi

Rabi is located ca 260 km south of Libreville (1.92°S, 9.88°E) where the altitude ranges from 30 to 80 m a.s.l. and the vegetation is comprised largely of lowland old growth rainforest. Overall, the CCI products v2 were in general agreement with the Lidar (acquired in 2015)derived AGB product and highlighted the spatial distributions of dense forest and degraded areas.

As with Mondah, a greater correspondence with the airborne Lidar-retrieved AGB was observed at Rabi for CCI Biomass 2017 & 2018 v2 than for 2010 v2 (Figure 5).

a)

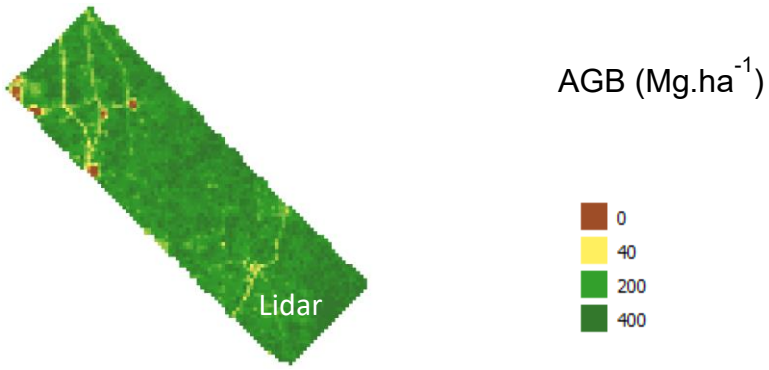

b)

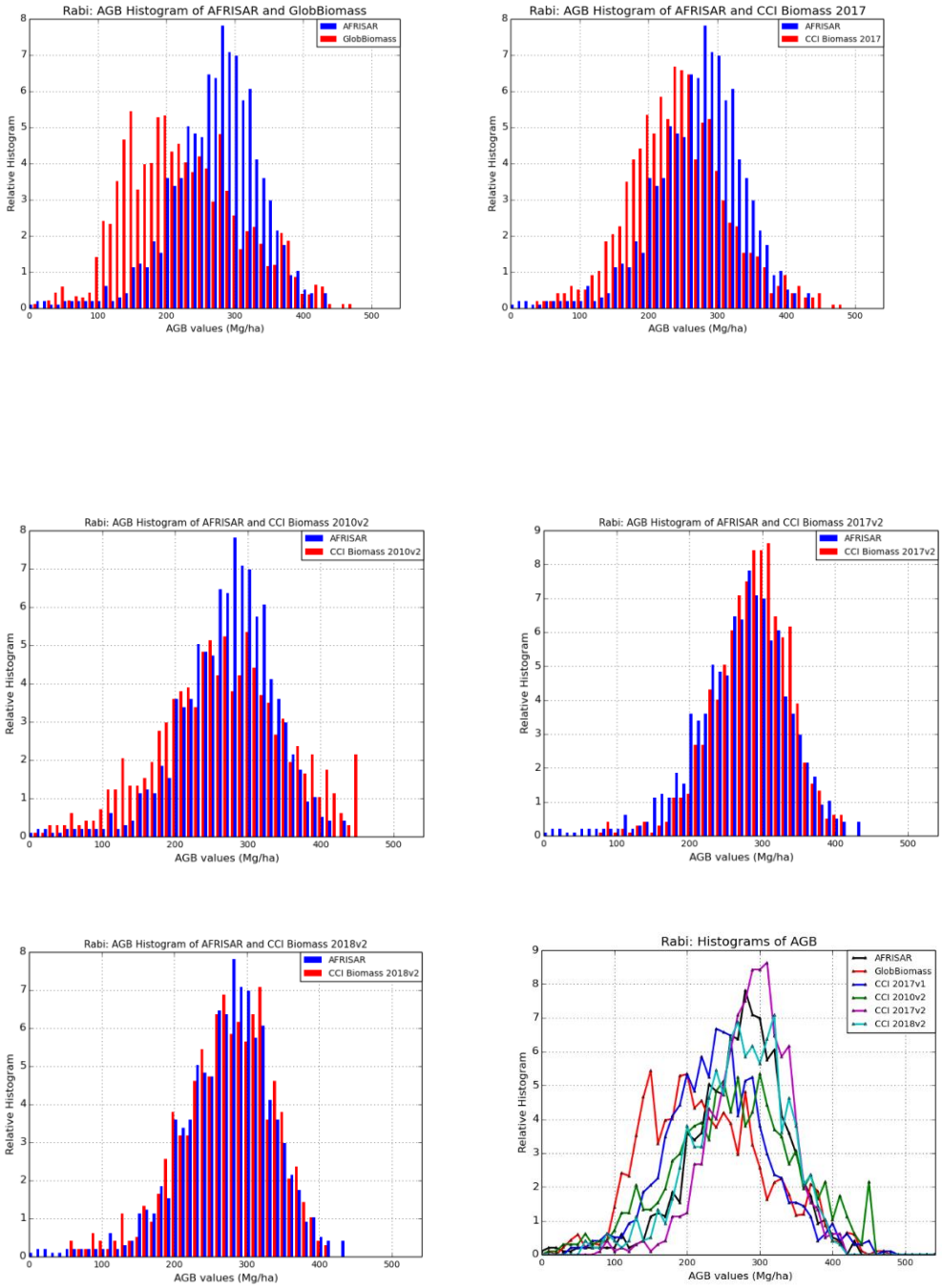

Figure 5: a) AGB maps derived from AfriSAR Lidar (top) b) Frequency distributions of AGB derived over Rabi, Gabon from airborne Lidar (blue) and from the 2010 GlobBiomass estimated AGB (red, top left), 2017 CCI AGB Year 1 (red, top right), 2010 CCI AGB v2 (red, medium left), 2017 CCI AGB v2 (red, medium right), 2018 CCI AGB v2 (red, bottom right), and all the different year's maps (bottom right).

French Guiana - Nouragues

Nouragues is located ~ 100 km south of Cayenne, French Guiana (4.06°N, 52.68°W). The terrain is gently hilly, with an altitude ranging between 26 and 280 m a.s.l. except in the northern part of the area where a granitic outcrop (inselberg) reaches 430 m a.s.l. Forest formations include high-canopy old-growth forest and lower-canopy forest formations, including periodically flooded forest dominated with palm trees, liana forest, and bamboo thickets. There are typically about 145 tree species per ha.

a) 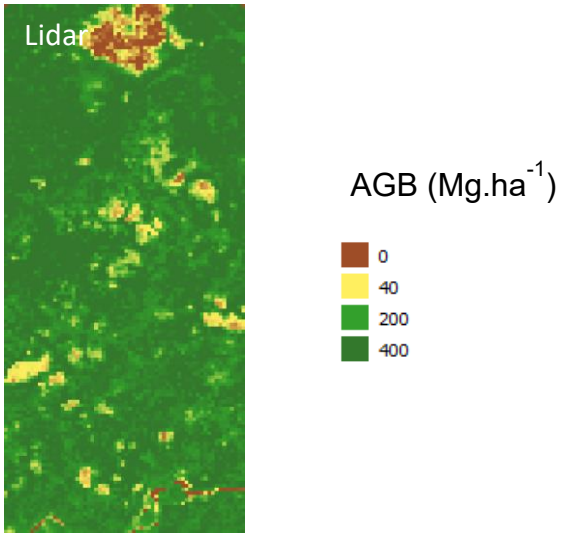

b)

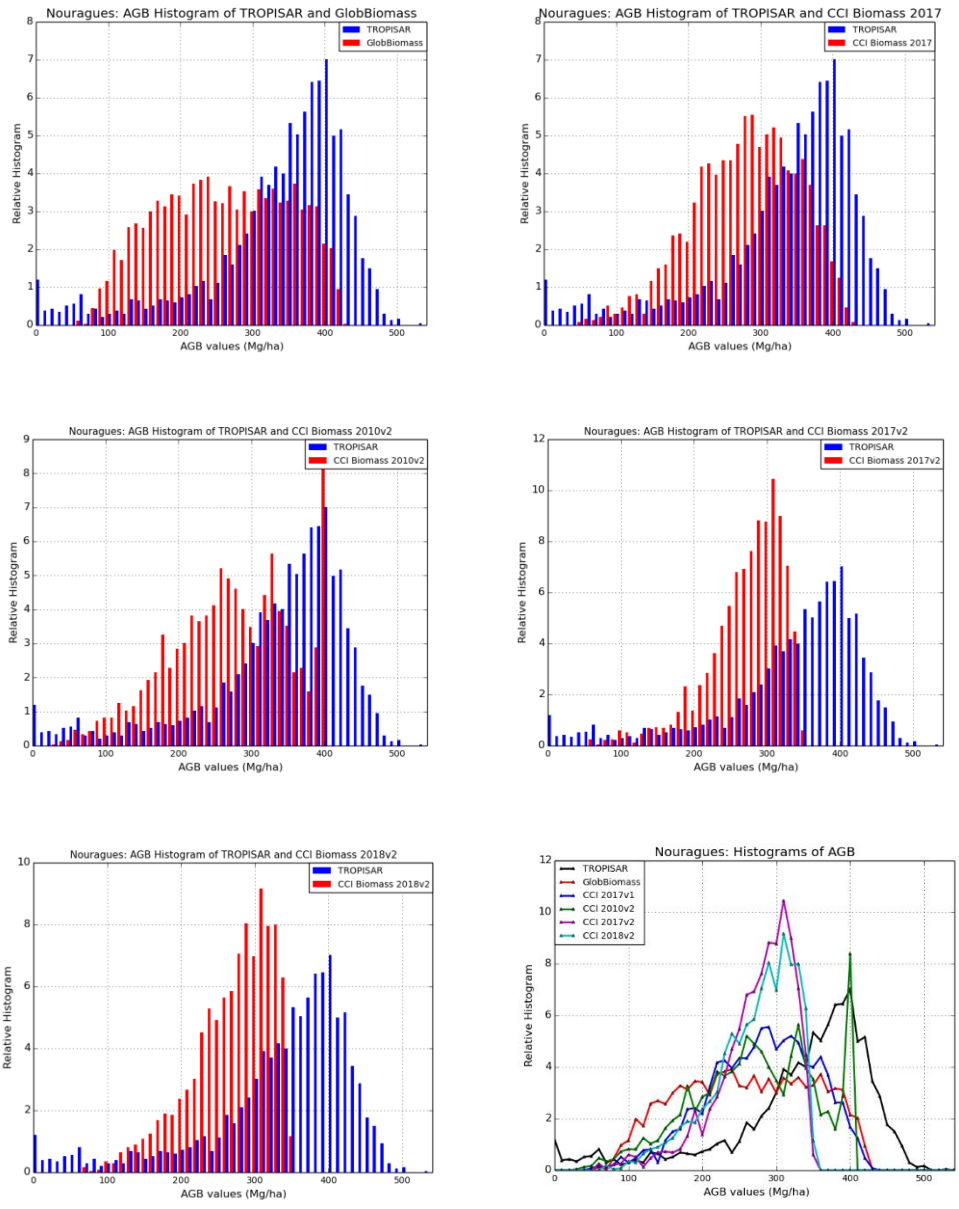

Figure 6: a) AGB maps derived from TropiSAR Lidar (top) b) Frequency distributions of AGB derived over Nouragues, Guyane from airborne Lidar (blue) and from the 2010 GlobBiomass estimated AGB (red, top left), 2017 CCI AGB Y v1 (red, top right), 2010 CCI AGB v2 (red, medium left), 2017 CCI AGB v2 (red, medium right), 2018 CCI AGB v2 (red, bottom right), and all the different year's maps (bottom right).

Overall, the distributions of the CCI products show discrepancy with the lidar -AGB map distribution: a) underestimation of AGB (abrupt end at 350 Mg ha^{-1} and 400 Mg ha^{-1} for 2017, 2018 v2, and 2010 v2); b) peaks of the distribution at 300 Mg ha^{-1} (compared with 400 Mg ha^{-1} of the reference); c) change in distribution from 2010 to 2017 cannot be explained by changes

in AGB in 7 years in this undisturbed forest. As for Mondah, the strong difference between 2010 and 2017 and 2010 and 2018 is a consequence of the different ALOS datasets: 1 HV image for 2010 (FBD mosaic) vs. about 10-20 HV images for 2017 or 2018 (FBD mosaic and K&C ScanSAR mosaics). In general, this comment applies to all high AGB forests in the tropics.

French Guiana - Paracou

Paracou is located ca. 75 km West of Cayenne (5.27°N, 52.93°W), where the altitude ranges between 5 and 45 m a.s.l. and the terrain is undulating. Mean tree species richness (ca. 140 species per ha) is comparable to that of Nouragues. The research station was established in 1984 in an area of undisturbed moist evergreen rain forest. The AGB ranges from 250 to 450 Mg ha^{-1}, the lower range of which corresponds to the plots partially degraded in 1984.

As for Nouragues, the CCI Biomass v2 maps show discrepancies with the reference distribution. a) underestimation of AGB (abrupt end at 350 Mg ha^{-1} for 2017, 2018 v2); b) peaks of the distribution at 300 Mg ha^{-1} (compared with 350 Mg ha^{-1} of the reference); c) change in distribution from 2010 to 2017 cannot be explained by changes in AGB in 7 years in this undisturbed forest.

a)

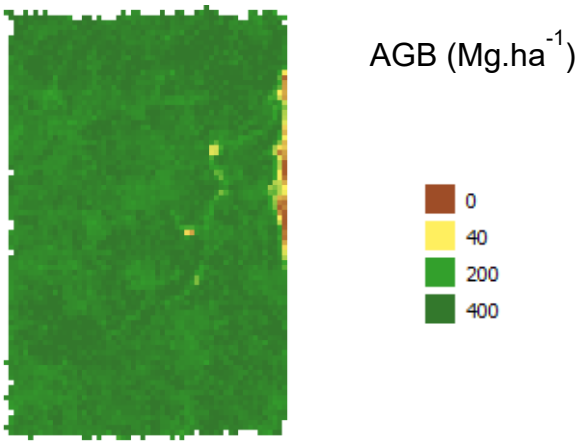

b)

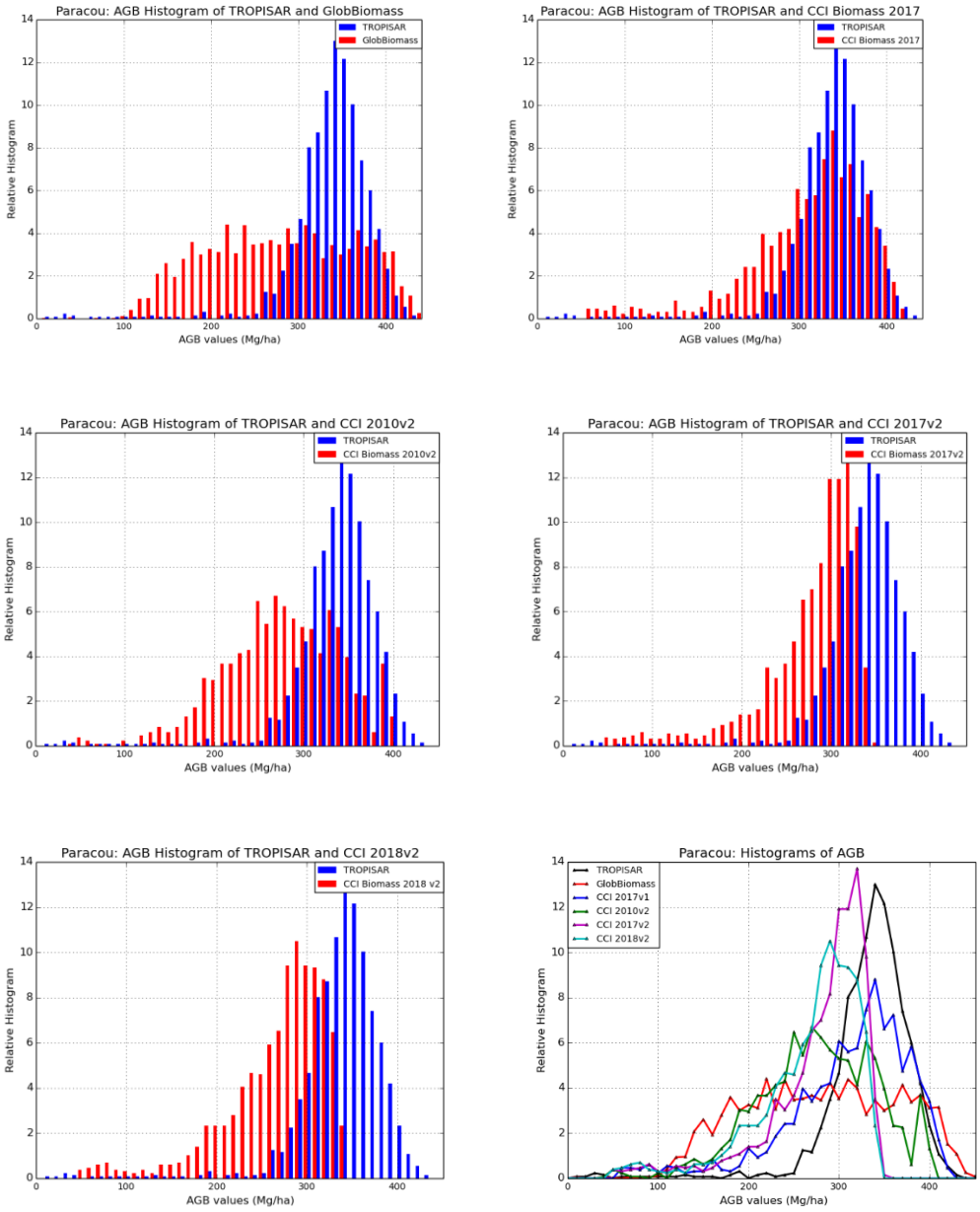

Figure 7: a) AGB maps derived from TropiSAR Lidar (top) b) Frequency distributions of AGB derived over Paracou, Guyane from airborne Lidar (blue) and from the 2010 GlobBiomass estimated AGB (red, left), 2017 CCI AGB v1 (red, right), 2010 CCI AGB v2 (red, medium left), 2017 CCI AGB v2 (red, medium right), 2018 CCI AGB v2 (red, bottom right), and from all the maps (bottom right).

2.1.2 AGB estimated from SLB and CMSKAL airborne Lidar

Two other airborne Lidar datasets were used, obtained from two international projects: Sustainable Landscape Brazil (SLB) and the Carbon Monitoring System (CMS) Kalimantan (CMSKAL) projects. The airborne Lidar data from both projects were processed by Nicolas

Labrière from EDB towards the production of Lidar-derived maps of AGB and associated uncertainty at 100m resolution.

The SLB dataset included tree inventory data (ca. 32,500 living trees from 31 inventories at 22 different sites scattered across the Brazilian Amazon) that were converted into plot-level AGB estimates and associated uncertainty, for a total of 625 plots ranging from 0.16 ha (40×40m square plots) to 1 ha (20×500m transects). The CMSKAL dataset provided directly plot-level information, for a total of 104 plots ranging from 0.1 ha (20×50m rectangular plots) to 1 ha (40×250m transects) covering both drylands (n=82) and wetlands (n=22).

Lidar-derived canopy height models (CHMs) were produced for all the point cloud data retrieved from the SLB and CMSKAL projects.

Mean top-of-canopy height (TCH) was either calculated within the footprint of each tree inventory plot from the relevant CHM (SLB) or provided for each inventory plot (CMSKAL), and power law models were built between plot AGB and TCH for drylands and wetlands separately (CMSKAL).

Applying these models to the Lidar footprints of the SLB dataset, AGB maps and associated uncertainty were produced. The total area in the SLB dataset covers ca. 820km2, from 286 different LiDAR footprints at 69 sites (68 in Brazil and 1 in Peru). The total area in the CMSKAL covers ca. 1,500 km^2 from 75 unique Lidar footprints (11 Lidar footprints were duplicates).

These datasets offer unique information for the assessment of the 100 m AGB datasets produced in the CCI Biomass project. However, most of the Lidar footprints consist in linear transects less than 200 m wide, i.e. a few pixels wide at the resolution of the CCI AGB datasets. Also considering that slight geolocation shifts can occur, this makes it difficult to compare the datasets at this resolution. Therefore, we chose to reproject the SLB and CMSKAL AGB estimates at a coarser resolution by averaging the values on a 0.01° (about 1 km) grid, as shown in Figure 8, and to conduct the comparisons at this scale.

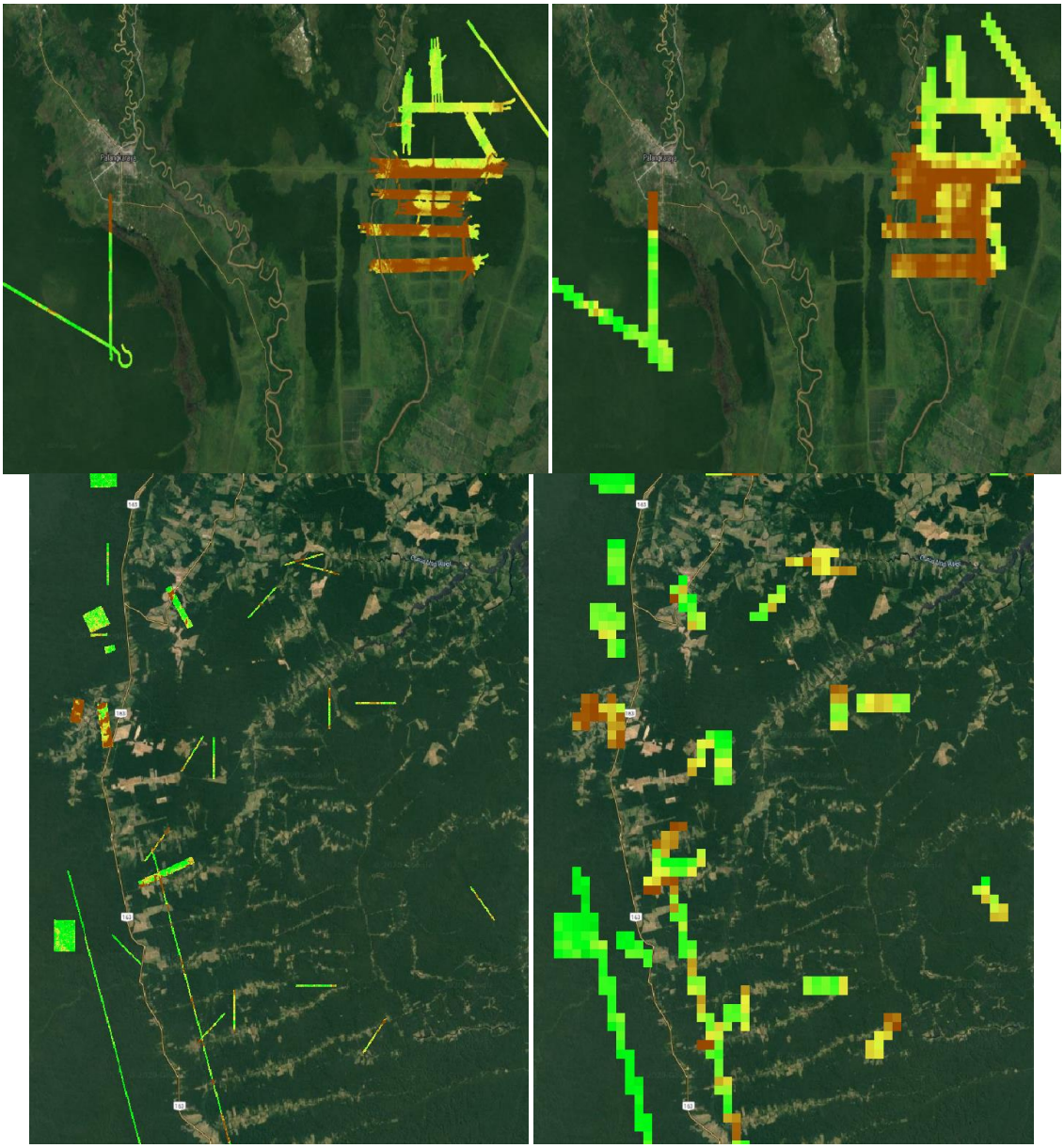

Figure 8: Subset of the CMSKAL (top) and SLB (bottom) AGB estimates from airborne Lidar data, at the resolution of 100m (left) and averaged at a 0.01° resolution (right).

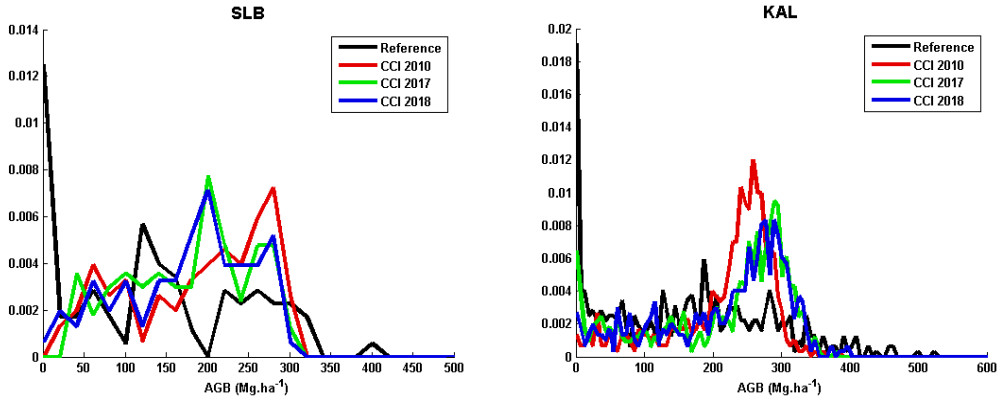

Figure 9: Histograms of the AGB estimated in the airborne Lidar and in the CCI 2010, CCI 2017 and CCI 2018 products over the SLB dataset (left) and the CMSKAL dataset (right).

The histograms in figures 9 show a) no strong correspondence between the Lidar-derived and CCI AGB v2 datasets; however, because of the possible mis-location error, it is difficult to explain the discrepancies found in SLB b) large variation between 2010 and 2017 and 2010-2018 CCI AGB; and this could not be explained by the AGB change in these regions.

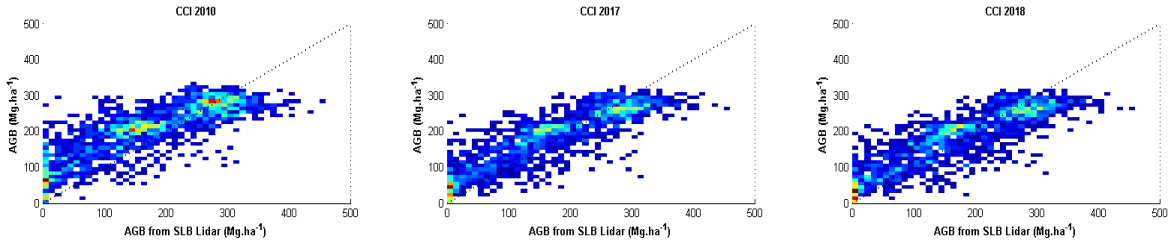

Figure 10: Scatterplots between AGB from SLB airborne Lidar and from the CCI 2010 (left), CCI 2017 (center) and CCI 2018 (right) products.

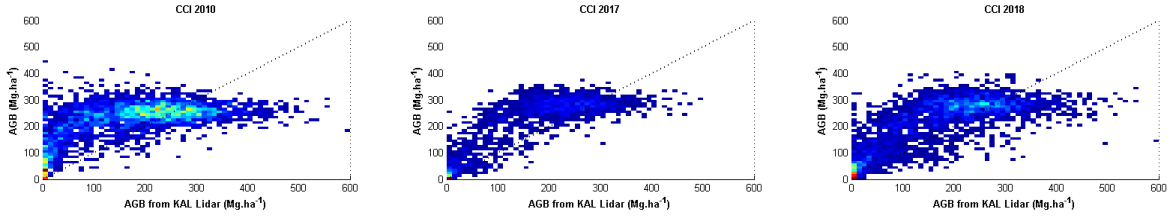

Figure 11: Scatterplots between AGB from CMSKAL airborne Lidar and from the CCI 2010 (left), CCI 2017 (center) and CCI 2018 (right) products.

The scatterplots show good comparisons between SLB datasets and CCI AGB v2 datasets, with saturation effect starting at 270-300 Mg ha^{-1}, and a slight over estimation of AGB before this value for 2010. For CMSKAL, the correspondence is less good, with overestimation in the low AGB range and saturation appears earlier (starting 150 Mg ha^{-1}).

2.1.3 Comparison with AGB map of RDC

Xu at al. (2017) generated a map of AGB for the Democratic Republic of Congo (DRC; Figure 13) by scaling (using a probability sampling approach) estimates from Lidar acquisitions over 432,000 ha of forest of different types (supported by 92, 1 ha ground plots) and using a combination of Landsat, ALOS PALSAR and Shuttle Radar Topography Mission (SRTM) data.

The comparison of the histograms of AGB of the DRC from the CCI Biomass products and Lidar product (Figure 13) highlights the bimodal distribution in the AGB associated with dense forests and grasslands/woodlands and the transition between these. However, in the SAR-derived products, the underestimation of the AGB of dense forests reduces the range of AGB in the 'transition zone'. The non-vegetated area (pixels of AGB=0) is underestimated in the CCI products.

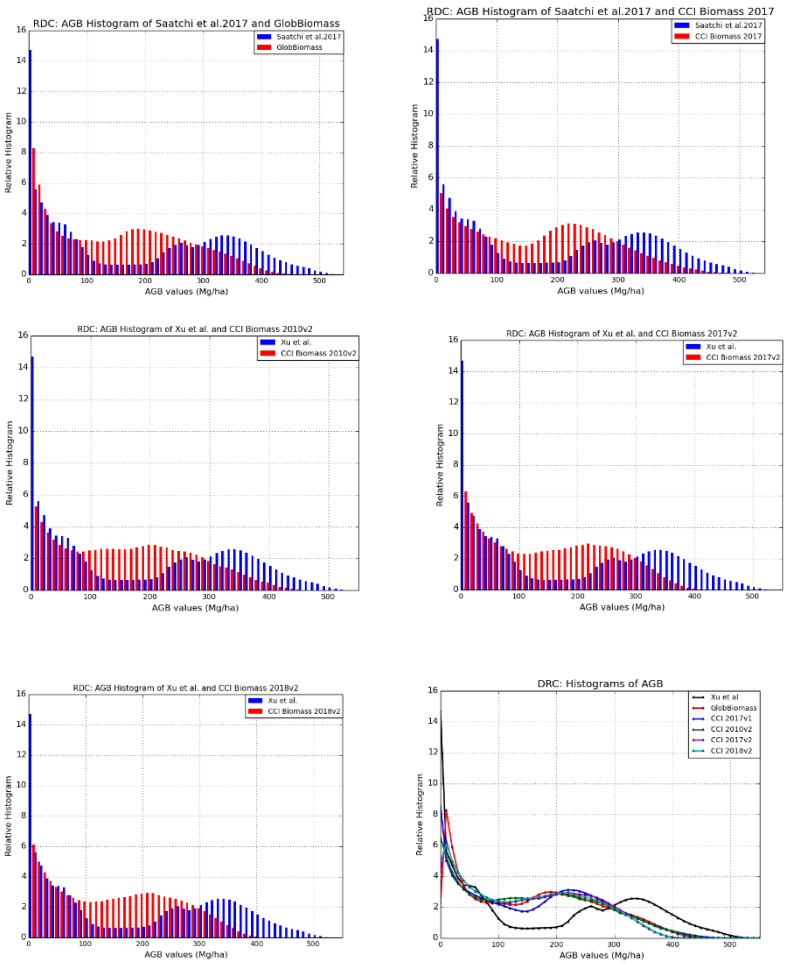

Figure 12: Frequency distributions of AGB derived over the Democratic Republic of Congo from the Xu et al. (blue) and from the 2010 v1 estimated AGB (red, top left), 2017 CCI AGB v1 (red, top right), 2010 CCI AGB v2 (red, medium left), 2017 CCI AGB v2 (red, medium right), 2018 CCI AGB v2 (red, bottom right), and all the AGB maps (bottom right)

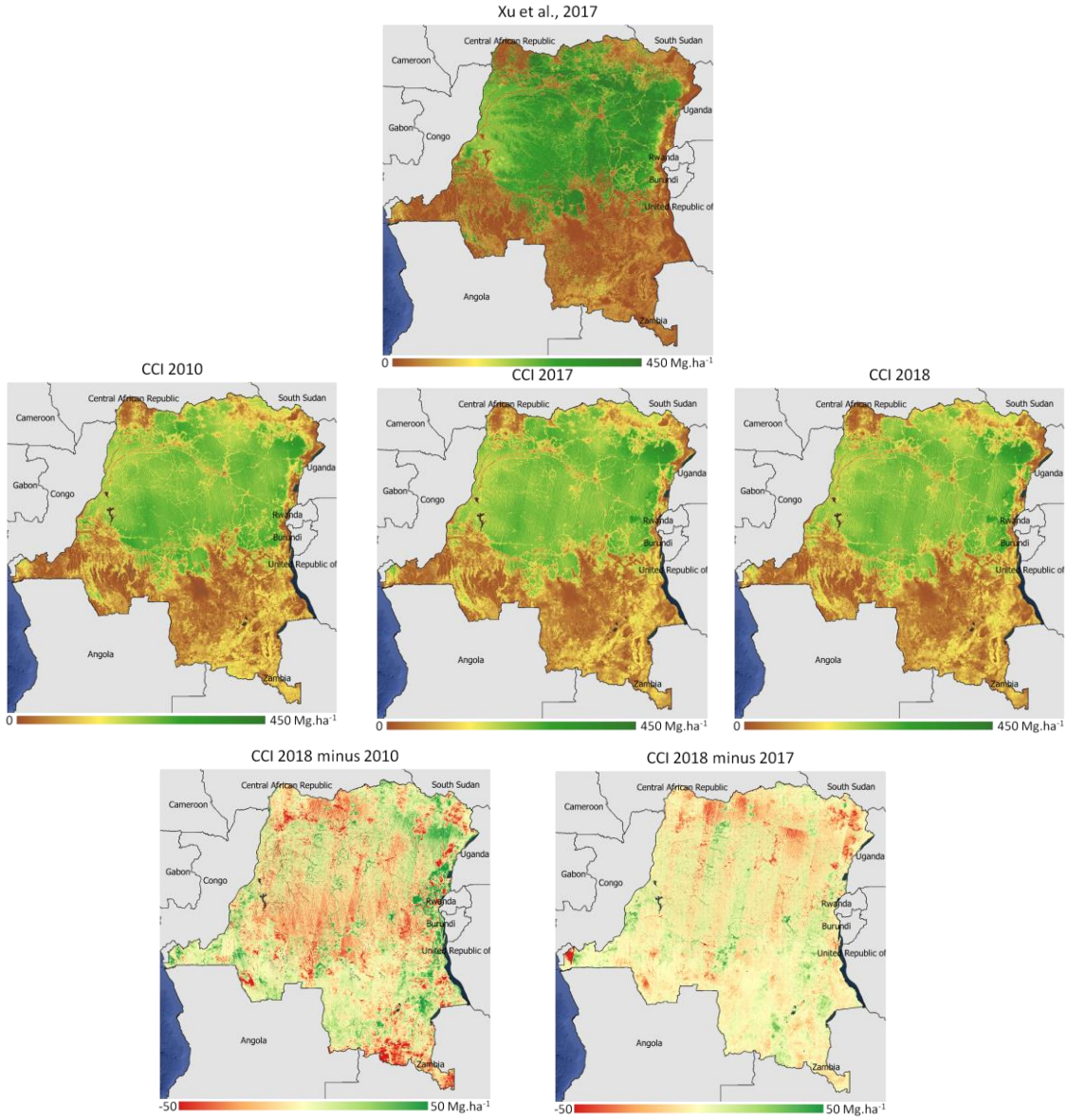

Figure 13: AGB maps of the Democratic Republic of Congo from the Xu et al., and from the CCI Biomass v2 for 2010, 2017 and 2018, and the AGB difference between 2018 and 2010, and 2018 and 2017. The color code is from 0 to 450 Mg ha^{-1} for the AGB maps, and from -50 Mg ha^{-1} to 50 Mg ha^{-1} for the difference maps.

The CCI AGB maps of 2017 and 2018 in Figure 13 show patterns caused by different satellite image strips (effect of incidence angle variation of the backscatter, and effect of changes in environmental conditions, in particular on the forest regions), which are less pronounced on the 2010 map. Compared to the Xu et al. (2017) map, the low AGB range (in brown in figure 13) shows similar spatial patterns, but the values are slightly over-estimated. The spatial patterns of forest AGB in the CCI AGB maps, are masked out by the stripping effects but show

lower AGB in the West and high AGB in the East. Compared to Xu et al. (2017) map, AGB values are underestimated in forest areas (in green).
The difference in AGB from the two 2018 and 2017 CCI maps showing increases in green and decreases in red, highlights that striping effects occur, and the 2018 and 2010 AGB difference maps map indicates some decrease in the Southern part of the forest area, and increase in the Easter part of the country. However, the strip effects should be reduced to highlight the AGB change.

2.1.4. Data from Ploton et al.,2020

In a recent paper, Ploton et al. (2020) introduced a Congo basin Forests AGB (CoFor-AGB) dataset that contains AGB estimations and associated uncertainty for 59,857 1 km pixels aggregated from nearly 100,000 ha of *in situ* forest management inventories for the 2000 – early 2010s period in five central African countries. The paper gives access to nearly 60 thousand 1 km resolution AGB estimates and associated uncertainty spread over contrasted forest types and environmental conditions in five countries from central Africa (Fig. 14). These estimates are based on the aggregation of c. 11.8 million measured trees in c. 192,000 field plots. The uncertainty on AGB estimations (8.6-15.0%) was found to be moderately higher than the error obtained from scientific sampling plots (8.3%).

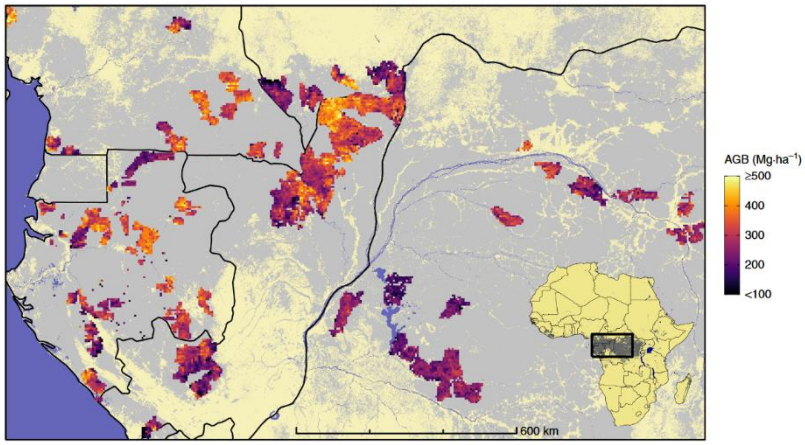

Figure 14: Distribution of study area in the Congo Basin and field data distribution of the datasets from Ploton et al., 2020 (Ploton et al., 2020. A map of African humid tropical forest aboveground biomass derived from management inventories. *Scientific Data*, *7*(1), 1-13.)

We compared the dataset with data by Xu et al., 2017, and CCI AGB v2 in 2010, 2017 and 2018. Figure 15 shows the resulting scatterplots and Figure 16 the histograms. The scatterplots indicate saturation of the CCI biomass beyond the range of 300-320 Mg ha^{-1}, which is not

observed with the datasets by Xu et al., 2017. However, Xu et al. seems to be consistently overestimated compared to Ploton et al. It is noted that Ploton et al, 2020 and Xu et al., 2017 used independent inventory and lidar data to form their datasets). The histograms show remarkable agreement in the patterns, with CCI AGB overestimated before 350 Mg ha^{-1} and underestimated beyond this range. Whereas the Xu et al., covers the entire range of AGB from Ploton, but with over estimation in the range of 300-400 Mg ha^{-1}.

If the Ploton et al. datasets are considered as reference, then :

- The CCI AGB show agreement in the pixel distribution in the range of 200-300 Mg ha^{-1}
- The CCI AGB show underestimation of the number of pixels below 300 Mg ha^{-1} and also underestimation above 300 Mg ha^{-1}
- The Xu et al., (2017) data are better related to Ploton et al., (2020) (r^2=0.22, as compared to r^2=0.04), but over estimated AGB in the range of AGB > 300 Mg ha^{-1}.

Despite the question about Xu et al., (2017) overestimation of AGB, its comparison with the CCI maps in the previous section is useful to illustrate the spatial patterns of AGB maps, covering different land covers: forest, savanna and wetlands.

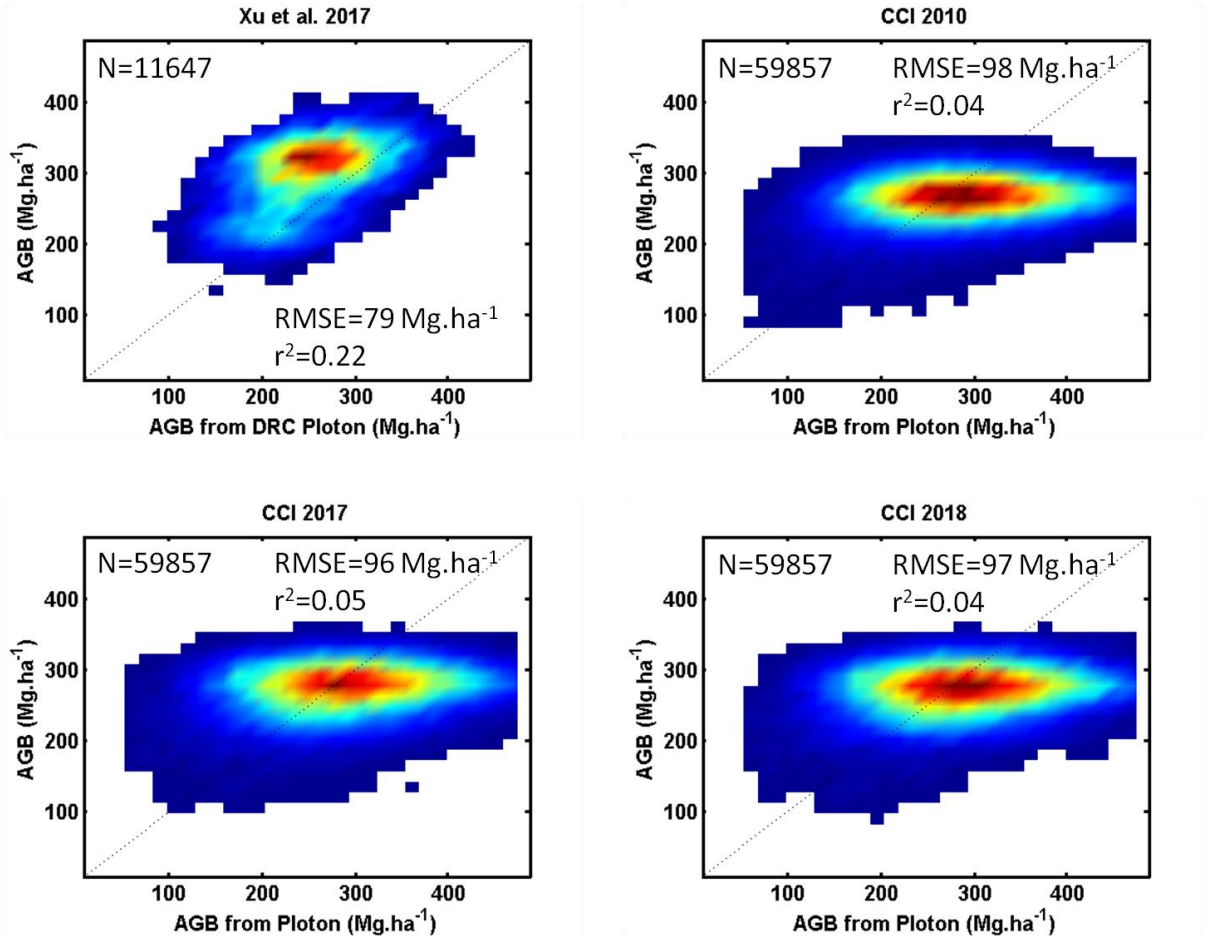

Figure 15: Scatterplots comparing datasets from Ploton et al., 2020 ; Xu et al, 2017; and CCI AGB v2 for 2010, 2017 and 2018. Note that the number of pixels in Xu et al. in RDC coincident with Ploton et al. Is smaller than with the CCI.

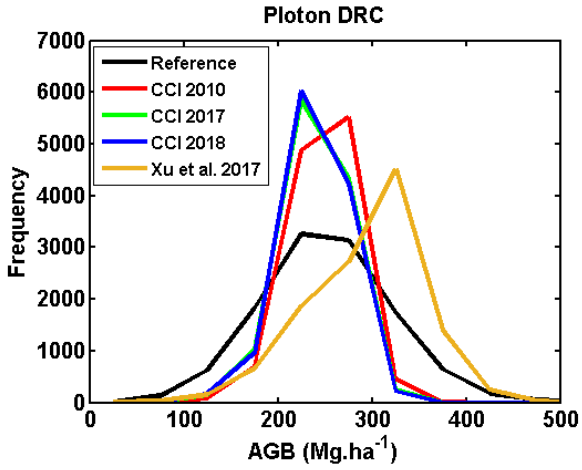

Figure 16 : Histograms of datasets from Ploton et al., 2020 (labeled Reference), CCI 2010, 2017 2018 and Xu et al. 2017.

2.2 Dry Tropics and Subtropics

2.2.1 Australia

The Terrestrial Environment Research Network (TERN) Australian Plant Biomass Library (APBL), through the AusCover facility (http://qld.auscover.org.au/public/html/field/) provided estimates of AGB (and associated errors) for 15,706 forest inventory plots distributed throughout all States and Territories and for all forest types (for the period up to 2015). AGB was estimated from individual tree measurements (over 2 million) generated by applying a standardized set of generic equations appropriate to Australian conditions (Paul et al., 2016).

In WP 1, EDB used data from the TERN network to produce AGB estimates from airborne Lidar acquisitions. Tree inventory data included ca. 28,800 living trees from 9 inventories at 5 different sites scattered across Australia. They were converted into plot- and subplot-level AGB estimates and associated uncertainty (the latter being produced for tropical locations only), for a total of 188 units (34, 1 and 153 of 1ha, 0.5ha and 0.25ha, respectively).

Similarly to what was done with the SLB and CMSKAL data, Lidar-derived canopy height models (CHMs) were produced for all the point cloud data retrieved from the TERN web portal.

Mean top-of-canopy height (TCH) was calculated within the footprint of each tree inventory unit from the corresponding CHM, and a power law model was built between plot AGB and TCH using all the 0.25ha units.

Applying this model to all Lidar footprints of the TERN dataset, AGB maps and associated uncertainty were produced. The total area covers ca. 370km2, from 13 different Lidar footprints at 13 sites (none of the sites were revisited).

Again, the data was re-projected to a 0.01° resolution grid.

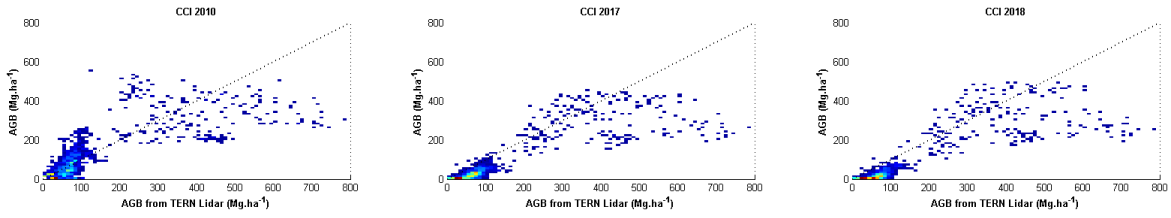

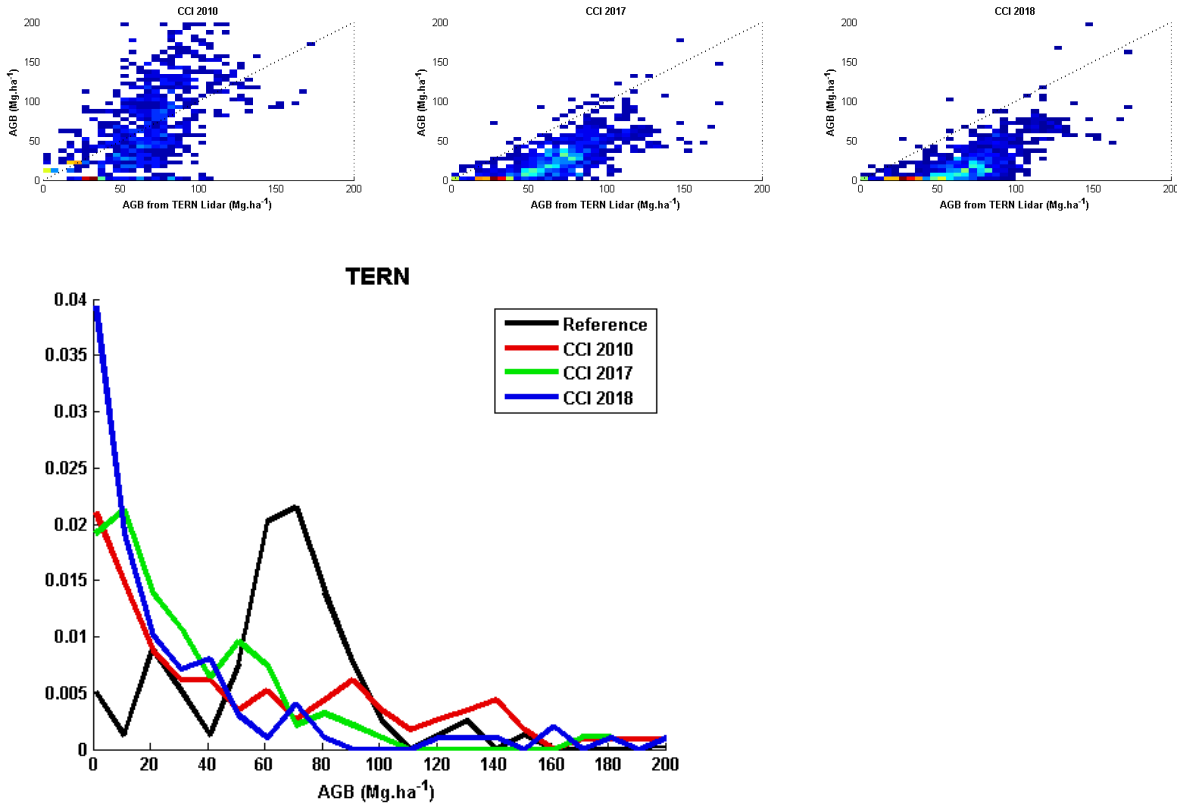

Figure 17: Scatterplots and histograms comparing TERN datasets and CCI AGB v2 for 2010, 2017 and 2018. On the first line, AGB is displayed in the full range, and on the second line, in the range from 0 to 200 Mg ha^{-1} , as for the histograms.

The scatterplots show saturation of AGB starting at 300 Mg ha^{-1}, and under estimation in the range < 100 Mg ha^{-1} for 2017-2018. The peak of reference histogram at 60-80 Mg ha^{-1} is not reproduced in the CCI histograms, which have the maximum distribution in the bare area (0 Mg ha^{-1}). The TERN inventories were conducted up to 2015, so that the difference in timing does not appear as an immediate cause of discrepancy in the lo AGB range.

2.2.2. Guinea-Bissau

1. CCI-Biomass above-ground biomass (AGB) maps

The 100 m spatial resolution CCI-Biomass AGB maps were queried to retrieve only the tiles covering Guinea-Bissau (West Africa). The spatial patterns and distribution of AGB values are different between 2010 and 2017 or 2018. AGB appear to be shifted towards lower values in 2017 and 2018.

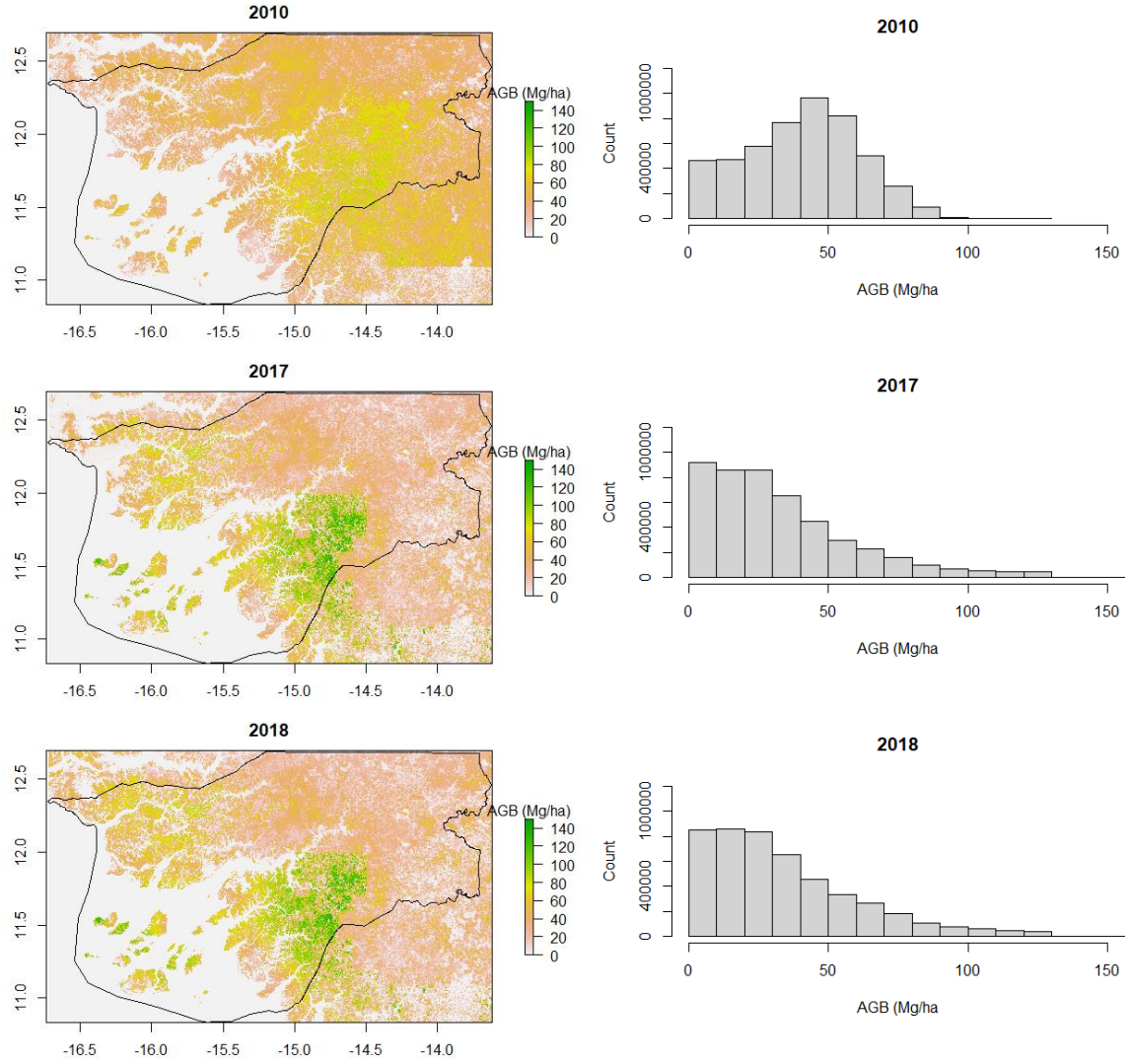

Figure 18: Maps and histograms of Guinea-Bissau extracted from CCI-AGB v2 maps 2010, 2017 and 2018.

2. Comparing pixel-level CCI-Biomass above-ground biomass (AGB) with in situ reference data

282 plots (~0.1 ha) were measured in Guinea-Bissau between 2007 and 2012. Diameter at breast height (DBH) and tree height (H) were measured and trees identified to the species level. Published allometric equations were used to estimate tree biomass as a function of DBH, H and wood density. These plots are used here to provide a high-level assessment of the AGB maps produced in the scope of CCI-Biomass. The comparison below is provided without time harmonisation between the AGB maps and the date in situ reference plots were measured. Furthermore, the CCI-Biomass 100x100 m pixel coincident with each plot is the basis for this comparison. The AGB retrievals from CCI-Biomass do not match those from small (~0.1 ha) in situ reference plots.

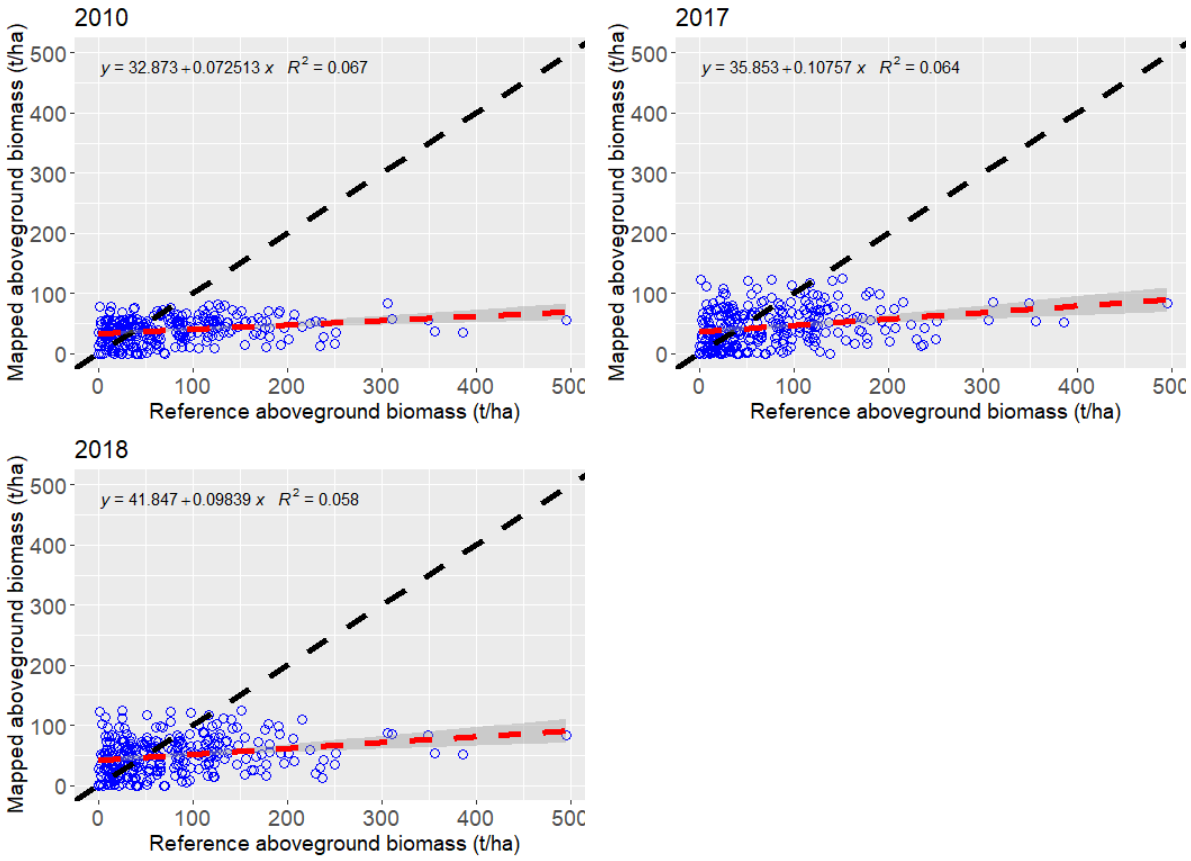

Figure 19 a: Scatter plots comparing reference AGB from 0.1 plots and CCI AGB for 2010, 2017, 2018.

3. Comparing CCI-Biomass above-ground biomass (AGB) retrievals with in situ reference data aggregated at 0.1 degree

In situ reference plots were averaged at 0.1 degree cells and only those cells with at least 5 plots were retained. The coincident AGB estimates from the CCI-Biomass maps were retrieved for those plots and averaged at the same 0.1 degree cells. As a result, of the initial set of 282 in situ reference plots, only 148 plots were retained, corresponding to 13 0.1 degree cells. The results of the comparison are shown below. Again, AGB retrievals from CCI-Biomass do not match those from in situ reference plots aggregated at 0.1 degree cells.

According to Gamma, the underestimation of AGB at high AGB could be understood that the algorithm is constrained by the AGB Max assigned to this region, which is of the order of 120 $Mgha^{-1}$.This is clearly lower than the max AGB measured at plots. Having constrained the retrieval to such low values of AGB explains the overall strong underestimation.

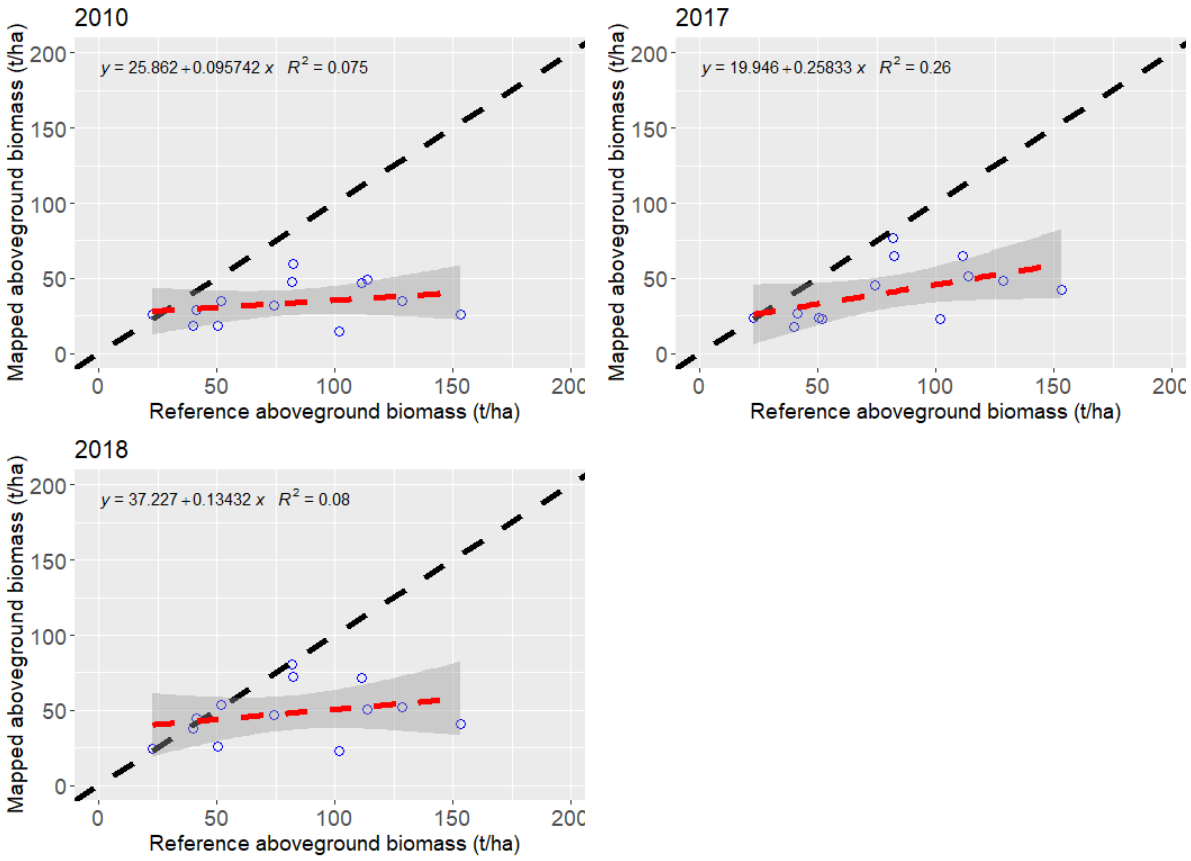

Figure 19b: Scatter plots comparing reference AGB from 0.1 degree cells and CCI AGB for 2010, 2017, 2018.

4. Comparing CCI-Biomass above-ground biomass (AGB) retrievals and corresponding standard deviation estimates

The plots below show the relationship between the AGB retrievals and the corresponding standard deviation estimates over Guinea-Bissau at full resolution (100-m pixels). There is clearly a trend of higher standard deviation with increasing AGB (green hexagons pointing to regions with higher density of values).

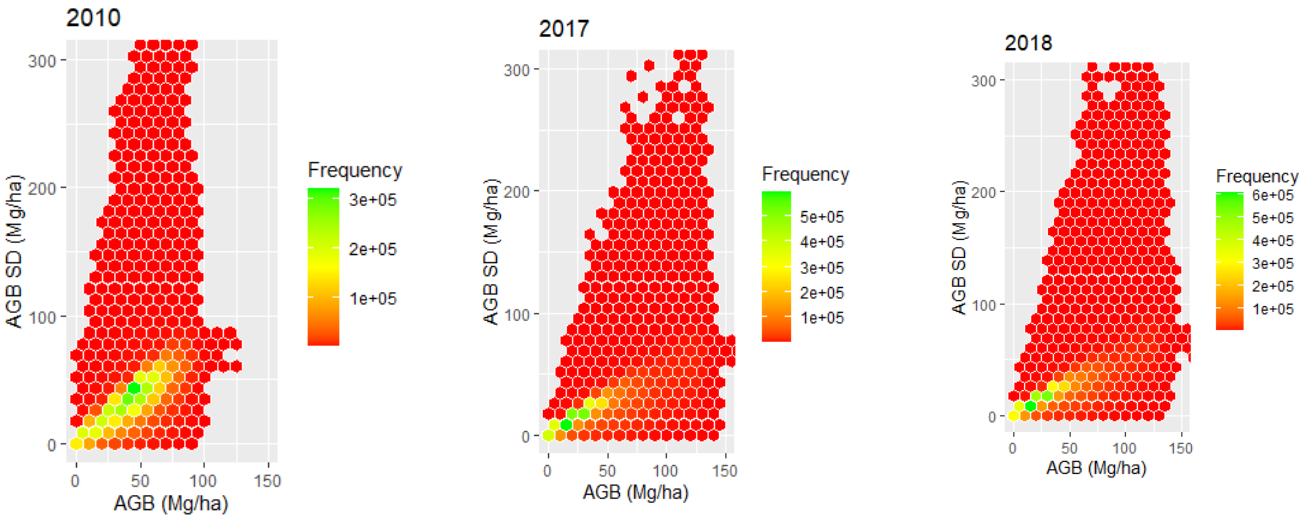

Figure 20: Standard deviation of CCI AGB (2010, 2017, 2018) versus reference AGB dor 0.1 degree cells .

2.3 Temperate and Boreal Biomes

2.3.1 Comparison with an existing AGB map (Sweden)

For the temperate and boreal biomes, a comparison was undertaken between an AGB map of the whole of Sweden (Nilsson et al., 2017) and the different CCI Biomass products. The reference map was a high-resolution national raster database (12.5 m × 12.5 m cell size) with forest variables produced by combining Airborne Lidar data with field data collected by the Swedish National Forest Inventory (NFI). Approximately 11,500 NFI plots (10 m radius) were located on productive forest land and inventoried between 2009 and 2013. These were used to create linear regression models relating selected forest variables, or transformations of the variables, to metrics derived from the Airborne Lidar data. The resulting stand level relative RMSEs for predictions of stem volume, were in the ranges of 17.2–22.0%. Compared to the CCI AGB v1, the histograms in v2 present a discrepancy in the distribution peak at about 100 Mg ha^{-1}, instead of 30-40 Mg ha^{-1} in the reference. AGB is underestimated in the CCI Biomass product at the low end of the range (AGB < 50 Mg ha^{-1}), overestimated in the 60-120 Mg ha^{-1} range, and underestimated for AGB > 150 Mg ha^{-1}. The time shift between the inventory data (2009-2013) and the satellite sensor data used cannot explain the observed discrepancy, in particular for 2010.

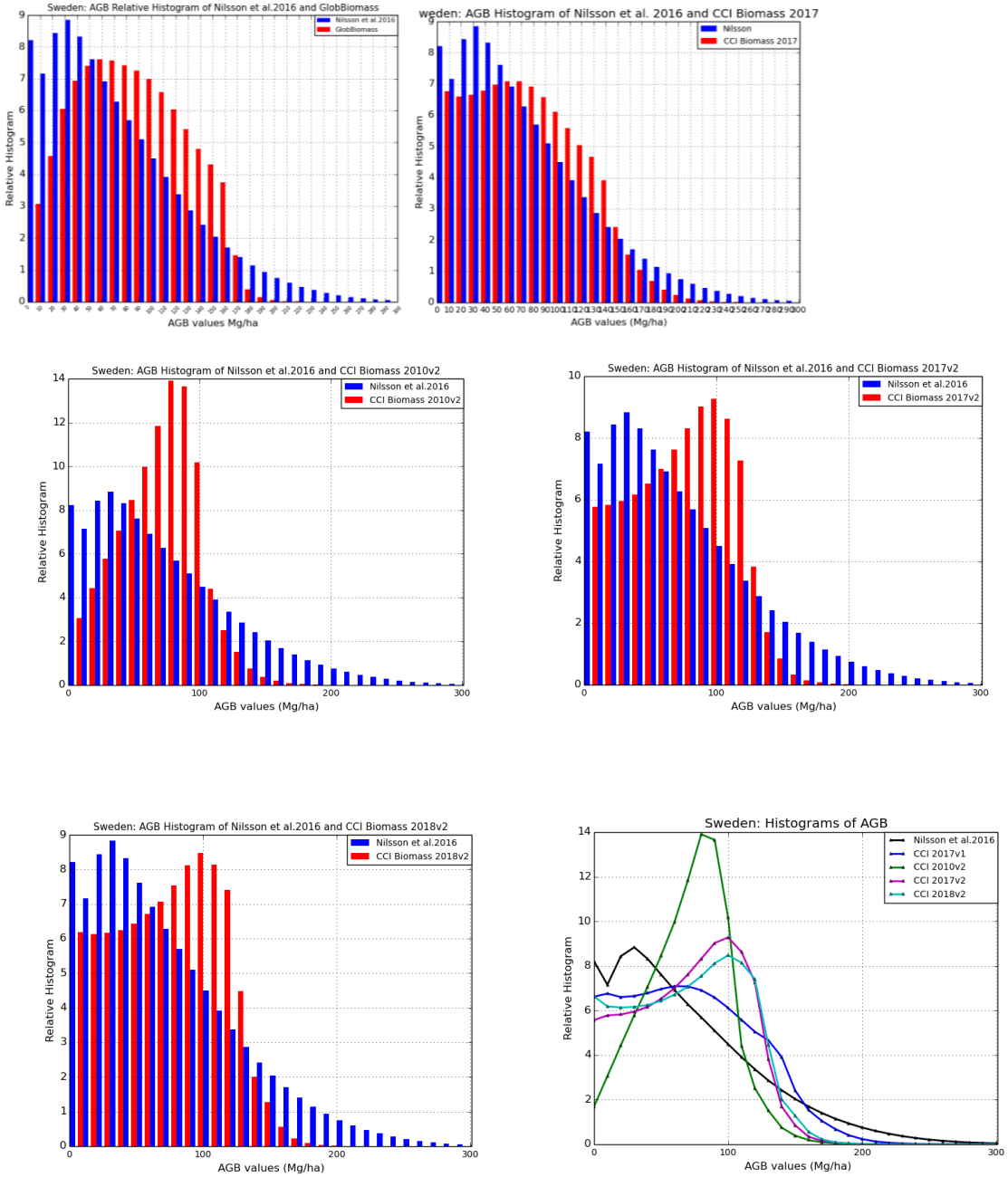

Figure 21: Top panels: Frequency distribution of AGB derived over Sweden from airborne Lidar(blue) and from the 2010 GlobBiomass AGB (red, left) and 2017 CCI Biomass AGB (red, right) products. Bottom panels: scatter plots of the GlobBiomass (left) and CCI Biomass AGB (right) vs the AGB from Nilsson et al. (2016).

2.3.2 Comparison with NEON airborne Lidar data (North America)

EDB used data from the National Ecological Observatory Network (NEON) to produce AGB estimates from airborne Lidar acquisitions. Tree inventory data included ca. 58,800 living trees from 126 inventories at 37 different sites scattered across the conterminous United States,

Alaska, Hawaii and Puerto Rico. They were converted into plot-level AGB estimates, for a total of 3,386 plots of 0.04 ha (20×20 m square plots).

Similar to what was undertaken with the SLB and CMSKAL data, Lidar-derived canopy height models (CHMs) were produced for all the point cloud data retrieved from the TERN web portal. Mean top-of-canopy height (TCH) was calculated within the footprint of each tree inventory unit from the corresponding CHM, and a power law model was built between plot AGB and TCH using all the 0.25 ha units.

By applying this model to all Lidar footprints of the NEON dataset, AGB maps and associated uncertainty were produced. The total area covers ca. 21,650km2 and includes over 125 unique Lidar footprints.

Again, the data was reprojected to a 0.01° resolution grid.

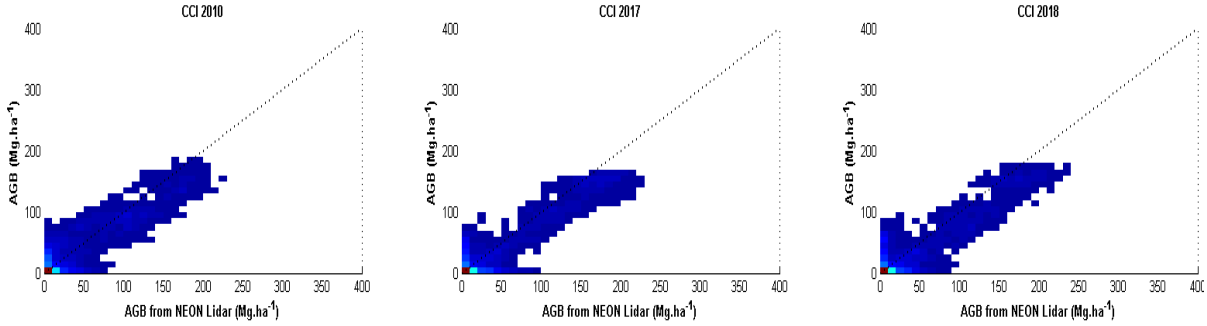

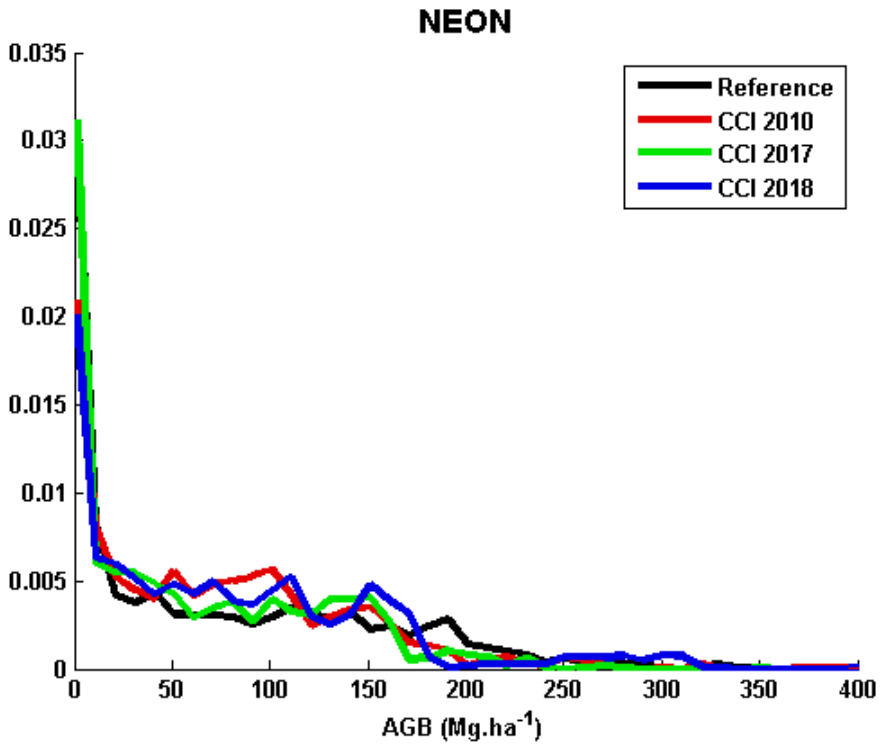

Figure 22: Scatterplots between AGB from NEON airborne Lidar and from the CCI 2010 (left), CCI 2017 (center) and CCI 2018 (right) products, and AGB distributions of the 4 products.

Overall, figure 22 shows good correspondence between the NEON and CCI AGB datasets. There is slight overestimation in the range of 20-170 Mg ha^{-1}, and saturation beyond this range.

2.3.3 Temperate forest, Wales

Approach

For temperate forests, field and airborne data for validation of AGB were less available compared to other biomes, with this partly the result of the sensitivity of data release by (semi-) commercial forestry organisations. However, for Wales (UK), recently released 10 m resolution land cover maps were available for 2017, 2018 and also 2019 at a national level from the Living Wales project (wales.livingearth.online). The classifications were generated using the Earth Observation Data for Ecosystem Monitoring (EODESM; Lucas et al., 2019, 2020) and according to the Food and Agriculture Organisation (FAO) Land Cover Classification System (LCCS; di Gregorio and Jansen, 2020). EODESM uniquely classifies and further characterises land covers by combining environmental descriptors (EDs) specified in the LCCS (e.g., canopy cover, height) or external to this. In this case, EDs were retrieved from time-series of Sentinel-1 SAR and Sentinel-2 optical data acquired in each year and, in some cases, external sources (e.g., Copernicus canopy cover).

The land cover maps for these three consecutive years (see example in Figure 23) were compared with the CCI Biomass AGB products for 2017 and 2018. This was undertaken to determine whether:

a) Detected changes in the extent of woody vegetation (primarily forests) corresponded with changes in AGB determined from comparison of the CCI AGB maps for these same years.
b) Areas where human activities identified in the Living Wales change products, such as clear cutting for timber harvesting, led to removal of all or the majority of woody (tree) vegetation and hence full loss of AGB.

In the latter case, the AGB in 2017 and standard error of the estimates are known (for 2017) and hence losses should be quantifiable if all or the majority of woody vegetation is removed (i.e., nominally 0 Mg ha^{-1} in terms of woody AGB). Gains in AGB over the one-year period between 2017 and 2018 were considered too small to be detectable given the low growth rates in the region. Land cover maps have not yet been generated for 2010 and so the comparison was not able to be undertaken.

Correspondence in areas of woody vegetation loss.

Areas of wood vegetation loss were identified where a) the FAO LCCS Level 3 category changed from (semi-)natural terrestrial/aquatic vegetation (woody) to any of the remaining categories (if present), namely cultivated terrestrial vegetation, artificial or naturally bare surfaces or (exceptionally) natural or artificial water or b) the area remained as (semi-) natural vegetation but the woody (tree) lifeform was replaced by primarily herbaceous or woody shrub vegetation.

The CCI Biomass estimates were compared initially by identifying areas where the AGB in 2018 was 50 % of that in 2017, and then extracting the corresponding AGB for 2017 to indicate the magnitude of losses in these areas. This was then repeated using thresholds of 60 %, 70 % and 80 % from which changes in the mapped area were compared (Figure 24).

The locations of areas where a 50 % loss of AGB relative to 2017 were similar to clear cuts detected through Living Wales, with these largely associated with the loss of coniferous plantations (including those dominated by Larch). In Figure 24, these are illustrated as having a loss of greater or less than 100 Mg ha^{-1}. When these thresholds were progressively lowered (i.e., to 80 %), more areas associated with a reduction in AGB were included. Where thresholds lower than 50 % were applied, clear cuts were not mapped or were reduced in area compared to the Living Wales maps.

By referencing the more detailed land cover map classes generated for Wales, an understanding of the reasons for low or no AGB was provided as follows:

a) When plantations are cleared, woody material is often left remaining on the ground (often arranged in rows) as are cut stumps and commonly for at least a year after felling. The exposed ground is also undulating, largely because of disruption of the ground during clearing operations and rearrangement of woody debris into rows. These factors combined lead to an exaggerated L-band and C-band backscatter, which can be misinterpreted by the CCI Biomass retrieval algorithm as a forest of relatively high AGB. This supports the conclusions obtained from analysis of L-band SAR data acquired over commercially harvested mangroves (Lucas et al., 2019) but also by previous studies (e.g., Stone et al., 0000).
b) In many areas cleared of forest, deciduous trees that are interspersed with the conifers are often not removed and, whist often scattered in distribution, their AGB contribution leads to an enhanced SAR response. Often, dense woody vegetation (e.g., heather or gorse scrub or successional (e.g., birch) species, which are often in the understorey and rapidly establish, which contributes a greater SAR backscatter, particularly at C-band.
c) As the landscape in Wales is complex, the 100 m area of the CCI Biomass map products may contain numerous land cover types with varying amounts and distributions of AGB. Therefore, the loss of AGB from pre-clearing activities (e.g., clear cutting) will only be reliable where forests are removed from the entire pixel. Where mixed pixels occur, multiple land covers and changes within these might occur and hence consideration needs to be given to the reliability of the AGB and error estimates for both dates.
d) Some of the observed differences may be attributed to the timings of the data used for the classification of land covers or retrieval of the AGB as these may differ depending on the sensor data used and particularly the L-band SAR integrated to form the global mosaics.

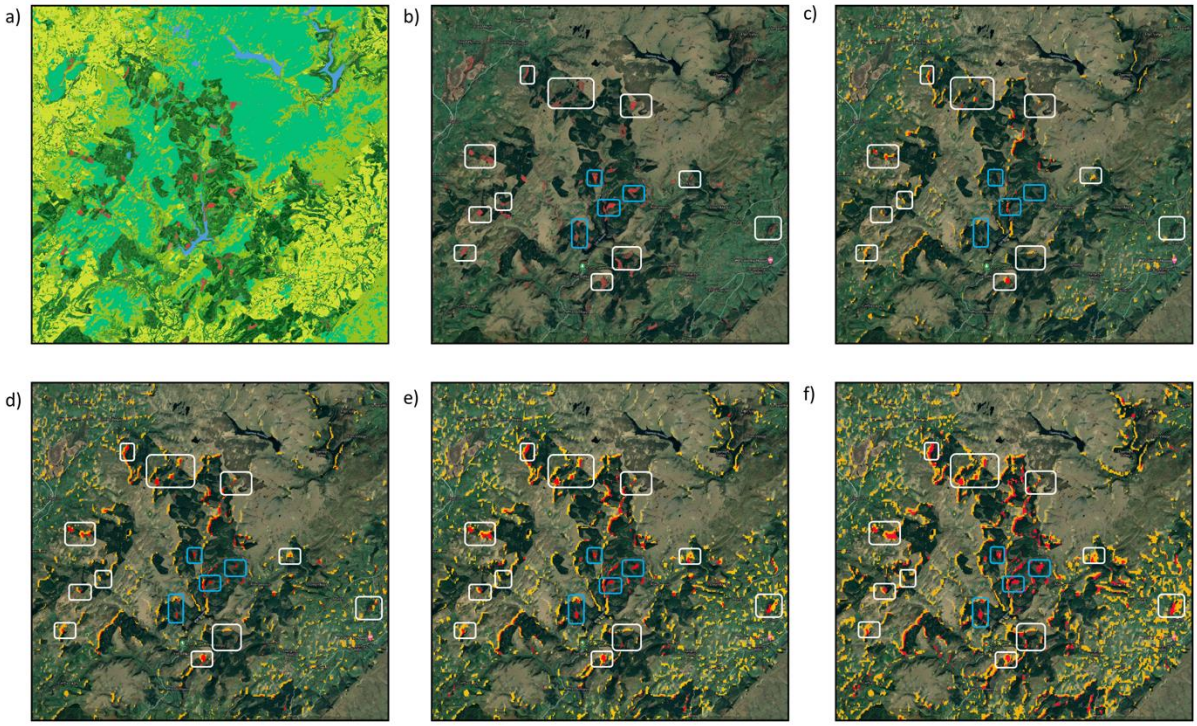

Figure 23. a) Land cover classification, Cambrian Mountains, mid Wales, b) forest clear cuts detected through comparison of FAO LCCS classifications for 2017 and 2018 and relative differences in AGB in 2018 as a proportion of the estimates in 2017; a) 80 %, b) 70 %, c) 60 % and f) 50 % with areas original above and below 100 Mg ha-1 in 2017 represented in orange and red respectively.

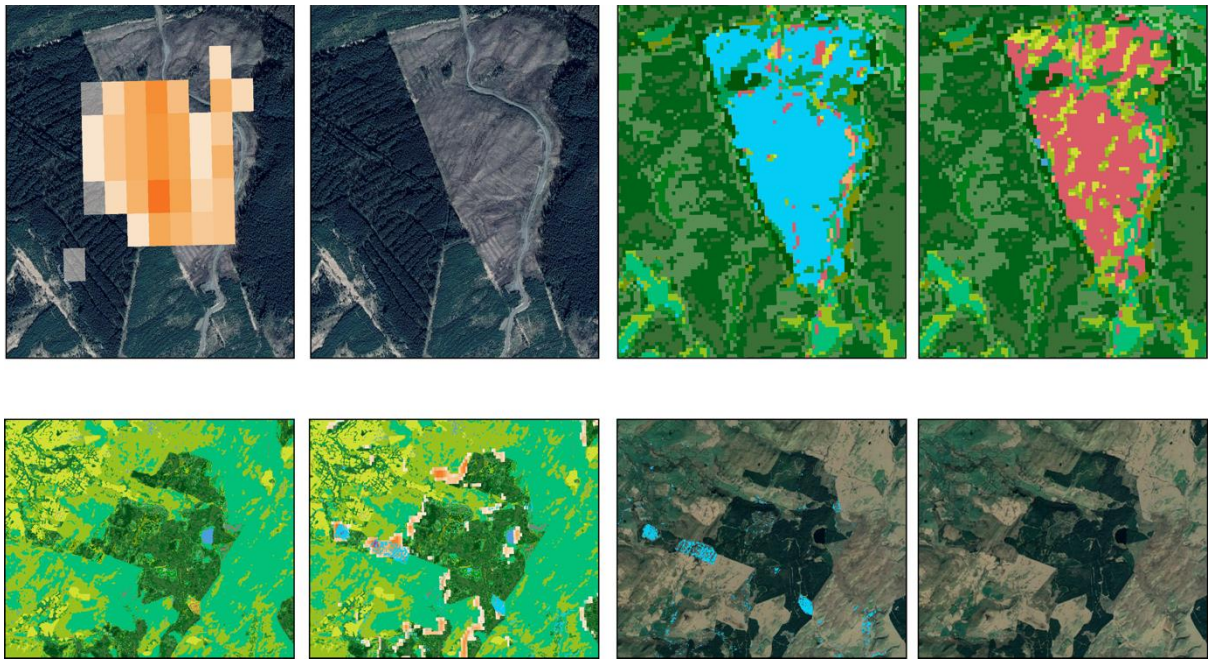

Figure 24. Examples of clear cuts in Wales, highlighting an area where a) differences in the AGB in 2017 and 2018 are large, with this being lower in extent that that b) observed in Google Earth imagery and c) determined

from comparison of the LCCS maps for 2017 and 2018. The classification of land covers in 2018 indicates the area of woody debris (red) but also a range of herbaceous and woody terrestrial and aquatic vegetation within the clear cut. Residual vegetation is common place after such events, with this including scattered trees or woody debris.

Discussions

Where to map AGB change.

For quantifying AGB change, consideration needs to be given to the natural events and processes and human activities that lead to change as these determine the extent to which AGB can be quantified and the associated uncertainties. For this, four scenarios of AGB change are suggested:

Changes between land cover types (extent)

In this case, changes often take place over a relatively short period (e.g., through deforestation, storms) and are detected through comparison of AGB between two consecutive years.

a. Losses of AGB from vegetation within a unit area such that none of the woody component remains (see Figure 26c as an example), with this taking place between the two times of actual or nominated measurement (e.g., by end of year).
b. Gains of AGB from an area with no or minimal AGB (e.g., 10 Mg ha^{-1}) to a larger amount over a selected time-period, which in most cases exceeds 1 year.

In the first case, changes can be detected through comparison of AGB between two consecutive years (i.e., 2017 and 2018), even if these are only differentiated by a year. However, confusion can arise where the land surface cleared of live woody vegetation contributes a signal that indicates its existence, even if the returned signal is reduced (e.g., woody debris left following clearance; as indicated earlier), or if woody AGB is lost from only part of the pixel area (i.e., resulting in a mixed pixel). In these cases, losses may only be detected where a defined signal associated with non-vegetated surfaces is recorded. They can also be detected over longer periods but this depends on whether the area cleared of woody vegetation remains as such or is replaced in subsequent years by plant growth. In the second case, such changes are likely to be detected only through comparison of AGB maps generated several years apart (e.g., 2010 and 2017 or 2018) as growth of sufficient magnitude for accumulating levels of AGB detectable by the algorithm is unlikely. The exception would be where large saplings that have been established beforehand are planted.

Where these situations are observed, the uncertainty of the AGB loss is associated with the uncertainty of the AGB in the year previous (in the case of i) or following (ii). A complication might be where the area of woody vegetation is replaced by urban buildings and infrastructure

as the SAR signal might be similar to woody debris left following forest clearing events or the ground remains quite rough (as illustrated in the case studies for Malaysia and Wales).

Changes within land cover types (amount)
In this case, woody vegetation remains as such between the two times of observations but changes in AGB are more gradual, with these taking place though.

I. Progressive accumulation of AGB, leading to a net increase between two time-separated periods.
II. Progressive loss of AGB, often through degradation processes, with these leading to a net loss over time.

In both cases, the detection of AGB change is compromised because uncertainties in AGB estimates from before and after changes needed to be considered, but this leads to complications particularly if both experience bias. These may be particularly exaggerated if the first AGB estimates is underestimated (e.g., as with mature tropical forests) and the second are overestimated (e.g., as commonly observed with lower biomass regenerating forests).

The conclusion therefore is to identify areas associated with each of these four scenarios. A fifth could also be considered. This is where the amount of change in the AGB of mature intact forests is within a range that is considered not to be detectable within the SAR signal and hence such areas can be removed from the areas where change events, processes and activities are taking place.

Conclusions

The main conclusions are

a) Woody debris following clearing of the forests compromises the detection of AGB change as the direction of change is confused (i.e., high SAR backscatter from cleared areas often indicates an increase (albeit exaggerated) in AGB.
b) Five primary change groups can be defined, which could be treated separately. These relate to either an increase or decrease in forest extent (and hence full loss or gain of AGB) or, if the extent remains the same, changes in AGB amount (through degradation or growth). Where forests are mature and remain undisturbed, and given the time-frames of comparison, such areas can also be separated.
c) When quantifying AGB and AGB change, consideration needs to be given to the area of the different land covers relative to the 100 m spatial resolution of the AGB product and the different change processes that are occurring.
d) AGB losses and their uncertainties can potentially be estimated if the natural event or process or human activity leads to a complete loss of biomass within and beyond the area of the 100 m pixel. However, were pixels are of mixed composition and multiple change processes are occurring, AGB change is more difficult to detect.

e) Where forests regrow on land where the AGB of woody vegetation is zero, the AGB estimates and associated uncertainty in the subsequent year are considered representative. However, changes in AGB of most forests are likely to require at least 5 years if they are to be detected using the CCI biomass algorithm, but this will vary depending upon the biome and associated climate, soils and topography (as examples).

2.4 Mangroves

Estimation of AGB

As previously reported in the PVSAR (Version 2) for the commercially harvested mangrove forests in the Matang Mangrove Forest Reserve (MMFR; Figure 25a), woody debris left on the ground following the clearing event leads to an exaggerated L-band backscatter that can exceed that of the mature mangrove forests (Figure 25b). In the previous 2017 AGB product for the MMFR, clear cuts where woody debris remain are associated with forests of high AGB, whereas the live AGB is typically less than 10-20 Mg ha^{-1} (if uncleared understorey trees or scattered individuals remain). This same effect remains in the CCI AGB products for 2010, 2017 and 2018 products and is likely to be evident in other regions (see Temperate forests). This effect could be accounted for by identifying areas with a relatively high combined C- and L-band signals in the first observation but substantially higher (by ~ 5 dB; Lucas et al., 2019) in the next, noting that this also occurs where forests are inundated (e.g., during freshwater or tidal flooding).

In the MMFR, The L-band HH and, to a lesser extent, HV backscattering coefficient is lower for mangroves compared to proximal tropical forests, largely because the large prop root systems of the dominant mangrove genus (*Rhizophora*) reduce scattering at L-band HV (although this is most evident at L-band HH). In the previous CCI Biomass product for 2017, this resulted in underestimation of the AGB of mangroves, particularly where *Rhizophora* species dominated (primarily in Southeast Asia and northern Australia). Whilst the extent of mangroves globally has been mapped through the Global Mangrove Watch (GMW; Bunting et al., 2019), differentiation of the dominant genera or species has not yet been undertaken but is one option to overcome the underestimation of AGB.

Detection of change in mangroves

Mangroves are highly dynamic ecosystems and the AGB changes rapidly because of natural events and processes such as storms, sea level fluctuations and temperature and rainfall (including flooding) variations. Human-influenced climate change is also exaggerating many of these pressures. Human activities also lead to changes, with these often associated with complete clearance (e.g., for urban development; e.g., sea and air ports, commercial harvesting).

Whilst AGB data are not widely available to validate changes in the AGB of mangroves, a number of natural events or processes and human activities are evident from time-series comparison of the CCI products, with these illustrating the diversity of pressures that are

occurring and the relative magnitudes of losses (either because of expansion or reducing in extent or change in amounts of AGB). Examples of pressures and impacts are presented in Figure 26, which highlights a) the loss of mangrove AGB between 2010 and 2017, sea level falls up to 30 cm combined with high temperatures and low rainfall led to dieback of mangroves along the Gulf of Carpentaria in northern Australia, b) strong winds associated with Cyclone Yasi led to damage to mangroves in Hinchinbrook Island on the east coast of Queensland and c) construction of infrastructure led to a loss of mangroves and associated AGB near Brisbane Airport. In each case, the CCI Biomass AGB products over time reflect qualitative observations of AGB change.

a)

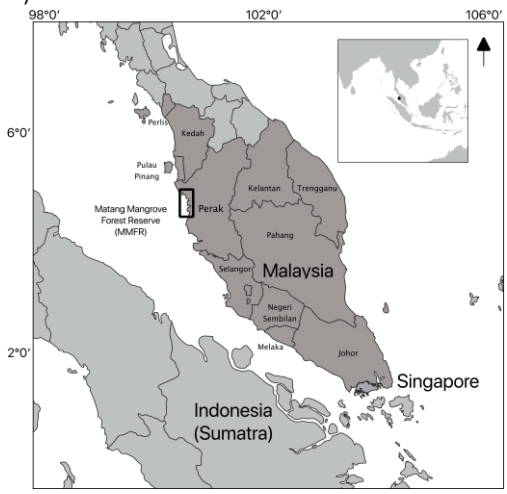

b)

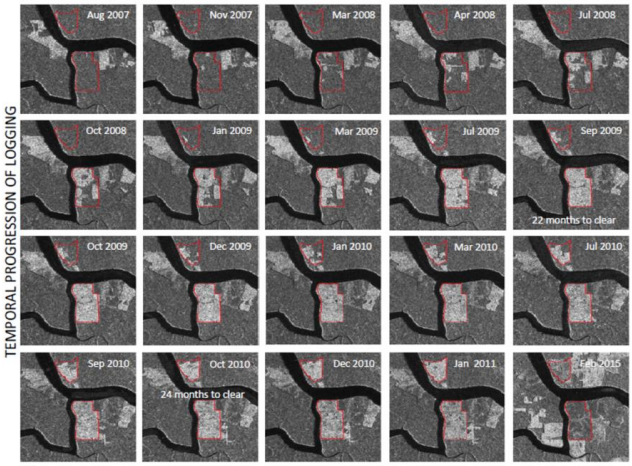

c)

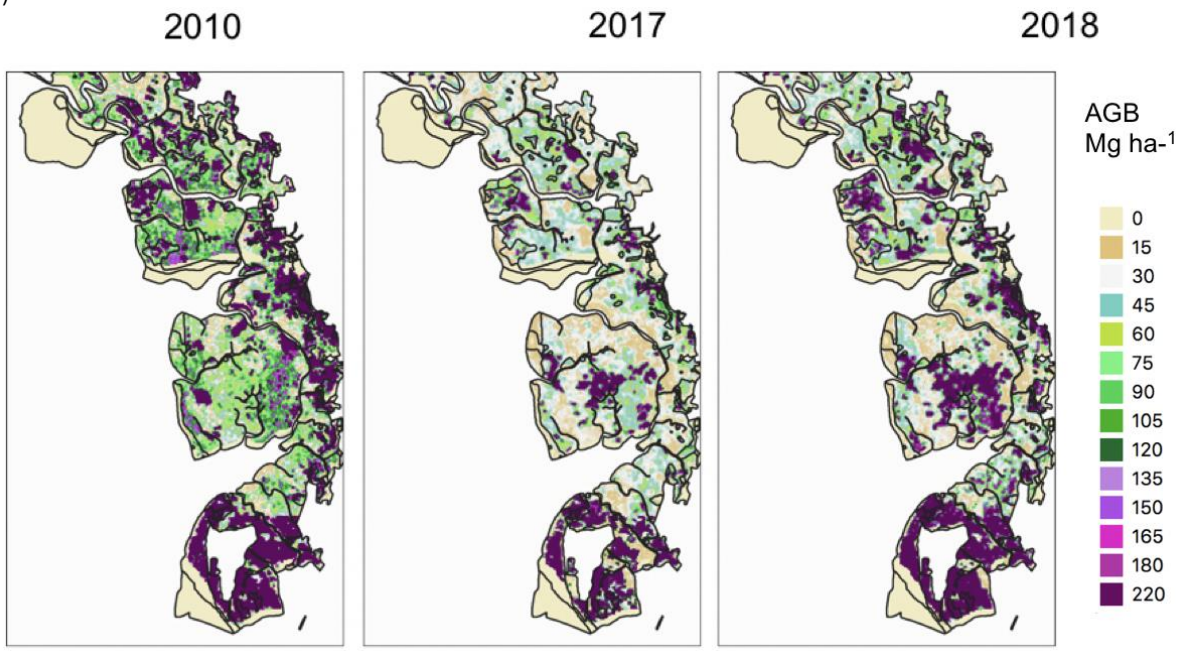

Figure 25. CCI AGB estimates for 2010, 2017 and 2018 for the Matang Mangrove Forest Reserve (MMFR), Malaysia with higher AGB associated with clear cuts (Lucas et al., 2019, 2020).

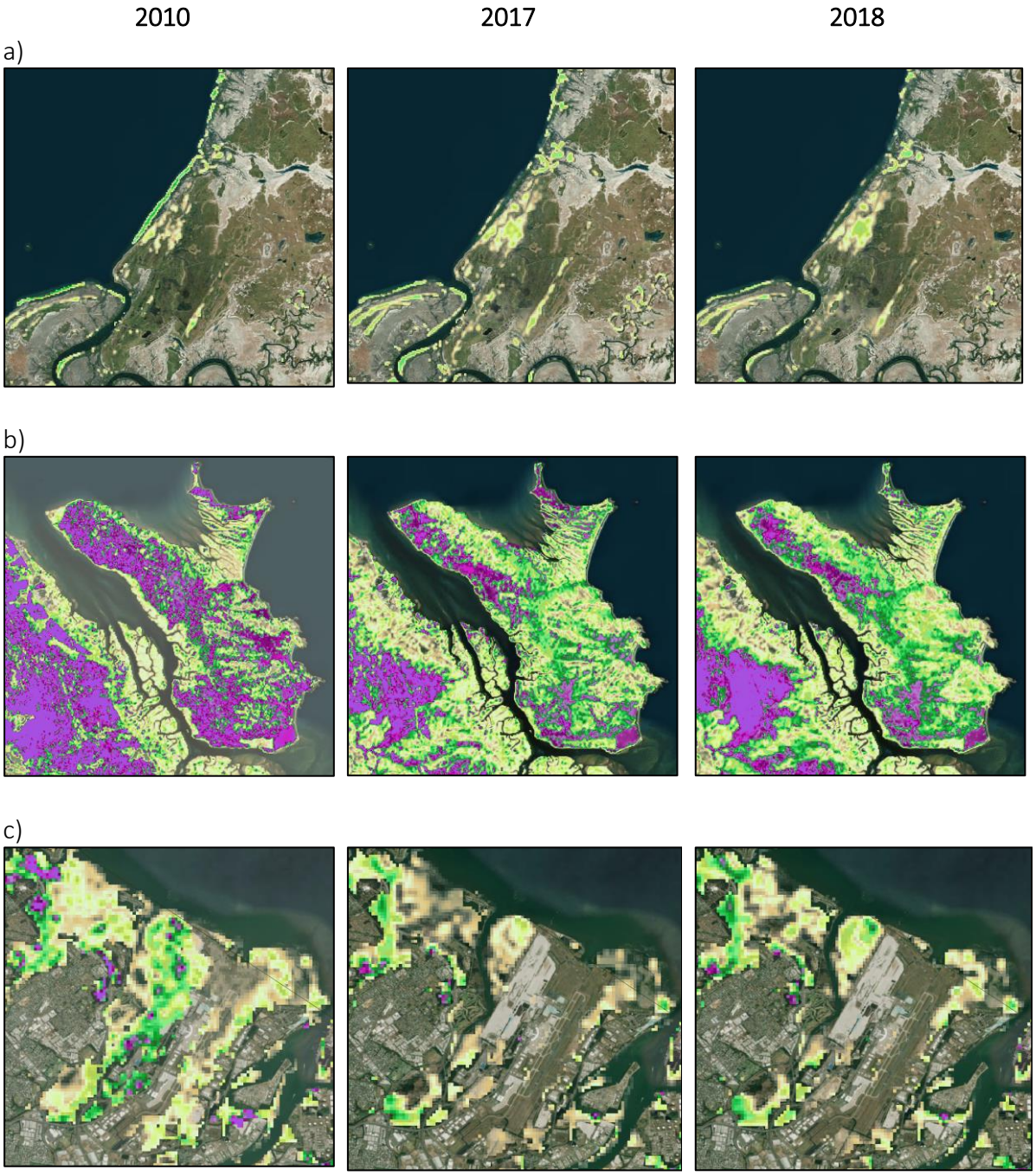

Figure 26. Changes in the extent or condition of mangroves in Queensland; a) the Gulf of Carpentaria (natural process), b) Hinchinbrook Island (natural event) and c) near Brisbane (human-activity), with these resulting in a loss of or changes in the amount of AGB. Background: Bing aerial imagery; see Figure 1 for AGB class legend.

2.5 Summary on the intercomparison

Overall, the CCI AGB maps v2 present better agreements with the Lidar-derived AGB maps than the 2010 and 2017 v1 maps. The inter comparison results can differ among datasets within a biome, and among biomes, but common remarks can be made as follows:

1. As stated previously in the PVASR Year 2, comparison of 100 m map products with plot data of <1 ha could be affected by the first type of error which is the mismatch between the map pixel and the plot location, due to geometric accuracy of the products and to the side looking SAR imaging. The error could be large for area with non-uniform AGB distribution. This is the case of sparsely vegetated areas such as dry forests and savanna in the inter-comparison, e.g. in Guinea Bissau and Australia.

   For this reason, AGB maps derived from airborne Lidar are more adapted to inter-comparison purposes.

2. For the low biomass range (i.e. < 30 Mg ha^{-1}) in all biomes, under or over estimation, and dispersion of AGB can have different causes:
   - the relative weight assigned to C-band data in the algorithm, to minimize the effect of changing soil moisture,
   - the patchiness of the vegetation which can introduce error into the AGB estimates, being less adapted to the assumption of a homogenous vegetation layer in the WCM algorithm,
   - the confusion with agriculture crop and plantation, for which model parameters derived for woody biomass could be less adapted,
   - the inclusion of the height from ICESat, which is not accurate for low and sparse vegetation

   One of the solutions could be to flag the low biomass range (i.e. < 30 Mg ha^{-1}) based on the criterium on the temporal variability of Sentinel-1.

3. The artefacts caused by image strips, as shown in the maps of RDC are perturbing when the maps are used at local/regional scale and also for the annual change, as for AGB difference in 2017 and 2018.

   The strips effects are explained by Gamma in WP3000 as follows:

The strips occur in 1) L-band mosaics (throughout the dense tropics) and 2) C-band Sentinel 1 (S1). In 1), this is a purely processing issue. JAXA mosaiced individual scans and then individual strips without accounting for intra-scan banding (ScanSAR) or different conditions at which images were acquired. In the future, one should strive for individual strips or, at least per-cycle mosaics. In 2), the S1 data used were processed by ESA with a wrong noise floor for some regions (Southeast US and China). The noise floor included in the metadata of the S1 has been improved recently by ESA. Unfortunately, due to budget issues, Gamma is not in the position to redo the whole processing of S1 data.'
We are expecting in the future to have better S1 data processing based on updated noise floor, and to obtain ALOS-2/PALSAR-2 data, either in per-cycle mosaics, or in individual strips data, to reduce the strip effect by dedicated processing in the algorithm. For the time being, it appears difficult to reduce these artefacts from the existing ScanSAR mosaics available to the project.

4. The abrupt AGB end of the AGB distributions in many sites (Mabounie, Mondah, Nouragues and Paracou) suggests that the maximum AGB set in the retrieval to avoid very high values of AGB from inversion, could be improved. The map of AGB max has been established using indications from different sources (inventory, plot data, local studies, etc.). However, the AGB max depends on many indicators (soil type and depth, solar radiation, precipitation, the length of rainy/dry season, etc.), and can change within short distances in a given biome (Paracou and Nouragues, ..., Lopé and Rabi).

   A relaxation of the AGB max could be tested, at least in tropical dense forests. If necessary, a further investigation on climatic and other drivers of the forest maximum biomass could be conducted by project partners.

5. The under-estimation of AGB at high AGB range (AGB> 300 Mg ha^{-1}) is primarily attributed to the use of L- and C- band backscatter data, with the retrieval algorithm not suitable for the high AGB values typical of many dense tropical forests. The potential contribution to access to AGB of tropical forest could be integration of a measure of canopy height (from ICESAT and GEDI) and the percent tree cover in the retrieval algorithm, as was suggested by the analysis of TC_{ProbaV} x H in the previous report PVASR v2. However, a limitation of this approach could also be found for very high biomass range because the height derived from ICESat and GEDI is not accurate for canopy heights above 30 m. (https://glad.umd.edu/dataset/gedi).

   The Year 2 algorithm introduced the Tree cover and the canopy height H in the canopy transmissivity T, expressed as $T=e^{-\alpha H}$ where α is the two way attenuation per metre

through the canopy and H is the depth of the attenuating layer. H is derived from ICESat in the algorithm, and this approximation may cause error in dense forest, where the attenuating layer depth can be smaller than the height retrieved from a Lidar.

In addition, the allometry used to link AGB to forest height AGB =a h^b, with a and b derived from ICESat and GlobBiomass estimates averaged to 0.25° is too coarse to take into account the spatial variability of allometry, and to be applied to pixels of 100 m . But according to Gamma, reversely, if the window to estimate allometry is reduced, there will be artefacts due often to too few Lidar samples.

6. Approaches for AGB change are addressed in the Mangroves and temperate forest, relying in changes of Land Cover. For quantitative estimates of AGB change, because of the different sources of EO data used to generate CCI AGB 2010, 2017 and 2018, it was not recommended to estimate AGB change from map substraction. Works are undertaken by WP300 and WP400 to make use of a consistent EO time series data for the epoch 2010-2020 to match them to a distorted estimated AGB . Candidate EO time series are L-VOD from SMOS (presented in PVASR-v1/2), and ASCAT. This will be topic of future reporting.

3 Suggestions of improvements

Despite the issues mentioned, the CCI AGB v2 products present a good compromise of what could be done given the limitations in EO datasets.
To improve the CCI AGB v2 products for the short term, solution some of the issues could be addressed.

3.1 Classification of areas of high AGB

The main shortcoming of the CCI products is the under-estimation of AGB for AGB < 300 Mg ha $^{-1}$. This has a strong impact on the estimation of the global Carbon stocks, and also on the amount of C loss associated to deforestation in high AGB forests.

The revisit of the data layers in the algorithm linked to Potential Maximum AGB is expected to improve the inversion result in high AGB regions. As for the allometry, it is expected that the relations between AGB and Canopy height need to be established for the product resolution (of 100 m), which could be challenging globally.

One idea is to make use of the dense time series of Sentinel-1 to explore other indicators than the radar backscatter.

Use of textural metrics from S1:

Our hypothesis is that areas with very high AGB could be distinguished by their textural features, created by the particular spatial distribution of emergent trees, tree crown, or crown (radar) shade from lower AGB areas. In a recent paper, Morin et al., 2020 investigated the use of texture metrics generated from optical and radar using a Grey Level Spatial co-occurence Matrix (GLSM) [61] to retrieve forest parameters from managed forests and plantations. Eight features were extracted: energy, entropy, correlation, homogeneity, inertia, cluster shade, cluster prominence, and Haralick correlation. Several window sizes have been tested and the best compromise was found with a window size of 7 pixels and 30 grey levels for the 10 m resolution images (Sentinel-1 and Sentinel-2).

We computed eight features: energy, entropy, correlation, homogeneity, inertia, cluster shade, cluster prominence, and Haralick correlation. Energy and entropy indexes measure the level of "order" in the image (repetitive patterns). Homogeneity and inertia indexes give an indication of the local changes in intensity. Cluster shade and cluster prominence indexes indicate the tendency of clustering of the pixels in the window. Correlation indexes measure the dependency of grey levels on those of neighbouring pixels (it means there is a relationship between two neighbouring pixels within the window). Energy, entropy, homogeneity and inertia are often strongly correlated. The final textural indexes we consider for the study were therefore homogeneity, correlation, cluster shade and Haralick correlation.

The method for estimating forest parameters has been tested in several forests in France. The Table below summarises the performance obtained in the Landes forest.

Table: Performance of indicators from EO data (Sentinel-1 backscatter and texture, Sentinel-2 , ALOS-PALSAR backscatter, SPOT 6), expressed in RMSE (%) in estimating forest parameters: best feature type, best to features, best 5 and 7 features.

	AGB	BA	DBH	Age	Density	Height
Best feature type	L-band 32%	L-band 29%	C-TI 26%	C-TI 27%	C-band 37%	C-TI 18%
Best two types combination	L + S2-BI-TI 28.0%	L + C 27.1%	C-TI + S2-BI-TI 21.2%	L + C-TI 18.6%	L + S2-BI-TI 30.7%	C-TI + S2-BI-TI 14.3%
Five types open access images	28.0%	26.9%	19.8%	17.4%	24.4%	13.2%
Seven types (Spot-6 included)	27.9%	27.0%	19.3%	18.6%	23.3%	13.7%

For AGB and BA (Basal Area), L-band backscatter is the best feature to use, but only slightly more efficient than the Sentinel-1 C-band backscatter or textural indexes (C-TI). The performances of the L-band decrease strongly on DBH, age, density and height. For these forest parameters, Sentinel-1 C-band textural indexes are the best indicators, followed by C-band backscatter, Sentinel-2 and Spot panchromatic textural indexes. Sentinel-1 SAR C-band data is therefore the best pick when using only one data type to detect forest structure parameters, which, in turn, is indicator of forest AGB.

In a preliminary work to test our hypothesis in tropical forests, the textural parameters have been computed over the Paracou test site, using 11 monthly images in 2019. Figure 27 shows

the results of Entropy, correlation, and homogeneity indices for 8 classes of AGB. The classes of interest for us are the 4 classes > 300 Mg ha^{-1}. The figure shows that textural information could be used to discriminate the high AGB classes, in particular the upper end of the range. Some interesting features are also to be interpreted, such as the large seasonal variation if the correlation indices and the high and stable entropy of high AGB area. Even though only the AGB class (e.g. from 400 to 450 Mg ha^{-1}) is detected and the quantitative information will be the mean value and range, without error bar, the information could be useful to complement the CCI AGB maps.

The work is pursued to analyse S1 data over other test sites. If confirmed, detection of high AGB forest could be developed using S1 textural metrics (e.g. using annual mean to increase the class separability).

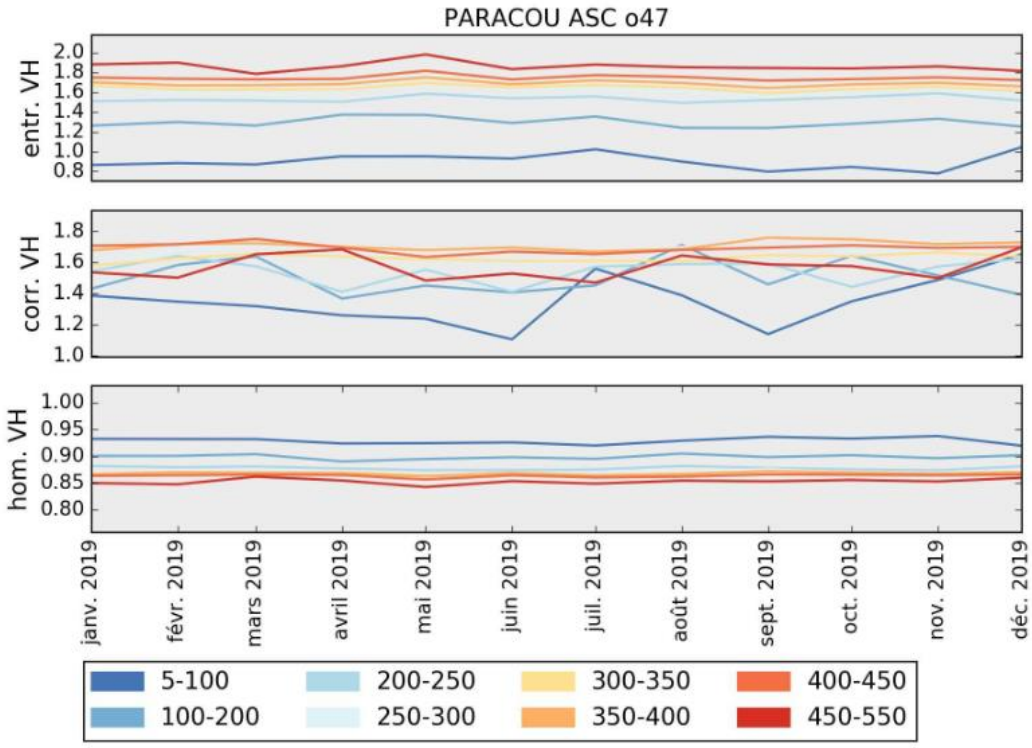

Figure 27: Textural indices (entropy, correlation, homogeneity) estimated from S1 images over Paracou

3.2 AGB changes

One of the objectives of the project is to provide quantitative AGB changes between 2010 and 2017/2018, using CCI maps at 100 m resolution.
Considerations have been discussed during CCI meetings and the CCI AGB change workshop concerning the methodology that could be used to estimate the AGB change between two epochs.
In general, the options which could be considered are:

- Absolute difference in maps of AGB
- Relate change in signal to a change in AGB
- Consider changes in AGB histograms to identify and quantify changes
- Combination with data time series spanning over the two epochs. Candidate data which show sensitivity to AGB are high temporal frequency/low spatial resolution SMOS data (through Vegetation Optical Depth).

For absolute difference in maps of CCI AGB 2017/2018 and 2010, several limitations have been identified. They are due essentially to the available EO SAR data used to generate the AGB maps.

- Different datasets and data density (number of EO data) have been used to generate the AGB maps of 2010 and 2017/2018
  - ALOS-PALSAR mosaics and ASAR for 2010,
  - Higher density of ALOS-2-PAlSAR-2 mosaics and Sentinel-1 for 2017/2018, (together with information derived from IceSAT data)
- Through the use of the current CCI algorithms, it is not possible to relate directly the change in a signal of ALOS-2-PAlSAR-2 and of Sentinel-1 to changes in AGB
- Variable differences in AGB (and in histograms) between AGB data (from LIDAR) taken as references and AGB from CCI 2010 and CCI 2017/2018 are observed in this report. It is not obvious to attribute a bias and standard deviation in AGB for each AGB map pixel, in order to assess the bias propagating in the difference map. Likewise, it is not clear how to provide an equation relating AGB to its bias and standard deviation in each map.
- The analysis undertaken in this report shows that saturation often occurs at AGB> 300 Mg ha^{-1} . In this case, change in high AGB region in tropical forest could not be detected using differences in AGB.
- Effect of image strips, caused by the use of PALSAR-2 mosaics data for 2017/2018 could not be reduced, causing artefacts in difference images 2018-2010 and 2018-2017 as shown in figure 13.

An alternative solution is relating the temporal trends from CCI with those obtained from time series of data (SMOS LVOD, ASCAT), under the assumption that the changes could be validated (or correspond to reality). The candidate time series data for 2010-2020 are SMOS and ASCAT,

with SMOS VOD at L-band having higher sensitivity to AGB than ASCAT at C-band (Fernandez-Rodriguez et al., 2018).

Figure 28 shows examples of monthly profiles of a number of pixels of LVOD (LVOD-IC v 105) for the 2010-2020 period in the Congo basin, and the map of Africa showing increasing or decreasing trend expressed in slope of the linear regression of the temporal profiles.

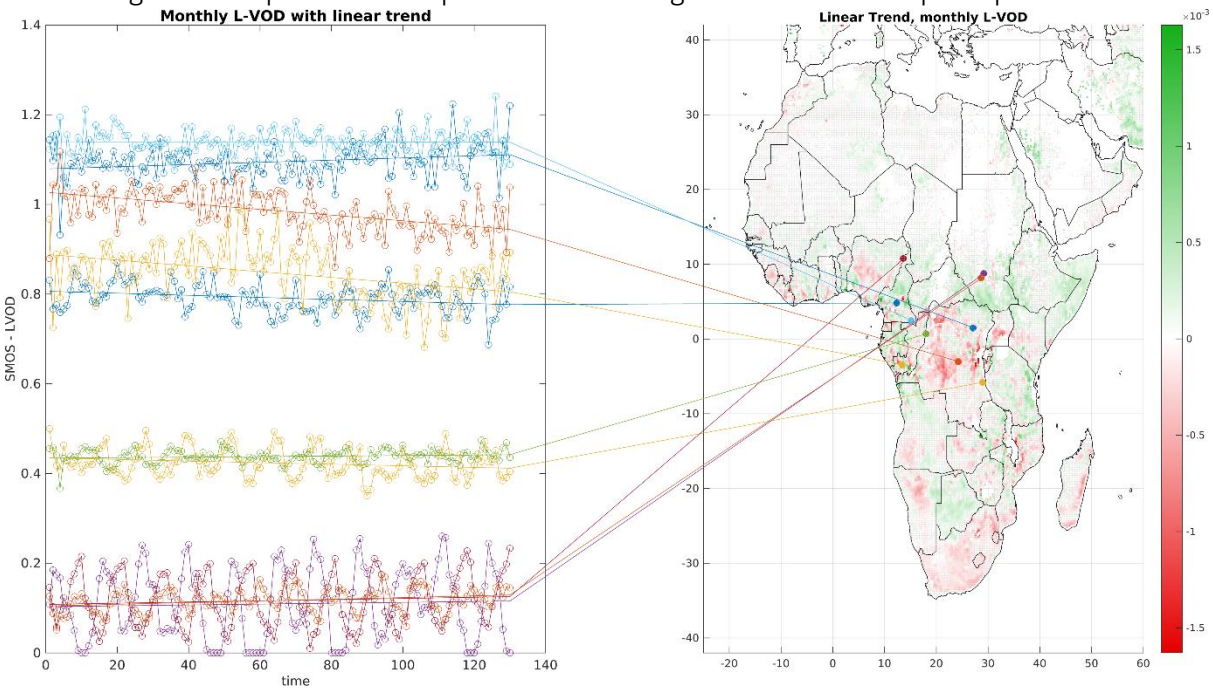

Figure 28: Right: map of L-VOD trend from 2010 to 2020, derived from L-VOD temporal profiles for each pixel. Red indicates a decreasing trend and green an increasing trend. Left: Examples of monthly profiles of L-VOD in the Congo basin. Time is expressed in months after January 2010.

In a first approach, the trend in L-VOD 10- year profiles as in Figure 28 will be used as indicator of the increase and decrease of L-VOD over the period.

For comparison with the map of 2008-2010 AGB difference from the CCI (as in figure 13), a map of difference in LVOD 2018 and LVOD 2011 in RDC has been created. In the latter map, wetlands or floods zone in the Congo basin which have interannual variability due to flood patterns were masked out.

Figure 29 shows a comparison of the CCI 2018- 2010 difference image at 1km pixel size and the 2018-2011 difference image from SMOS VOD, at 25 km pixel size. In the two images, Red colour indicates a decrease and green colour an increase in AGB or in VOD.

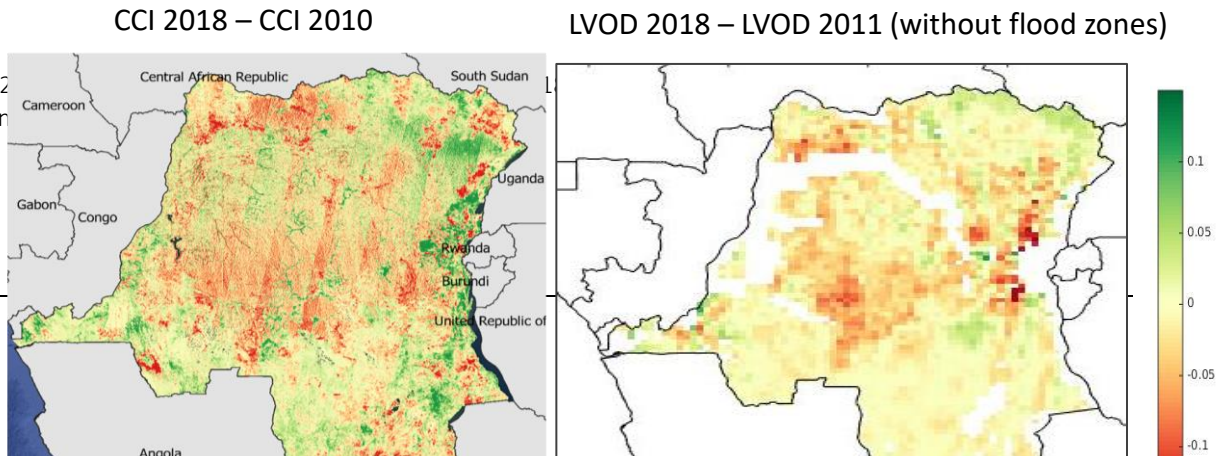

Figure 2
LVOD in

Figure 29 shows that there is some correspondence between the two maps for the large (red) region in the centre, and in the North West part of RDC. However, it is difficult to isolate the AGB changes in CCI maps from the changes caused by the image strip artefacts.
As stated above, the strip artefacts are caused mainly by the ALOS-2 PALSAR-2 ScanSAR mosaics for 2017 and 2018. It would be possible to reduce the strip effects only if we could access to strip data.
An attempt has been made to assess the reduction of strip effects with degrading map resolution. Figure 30 shows the maps of 2018-2010 AGB differences, derived from individual maps at 1 km and 10 km resolution. At 10 km, the strip effects are still visible in tropical forests in the Congo basin.

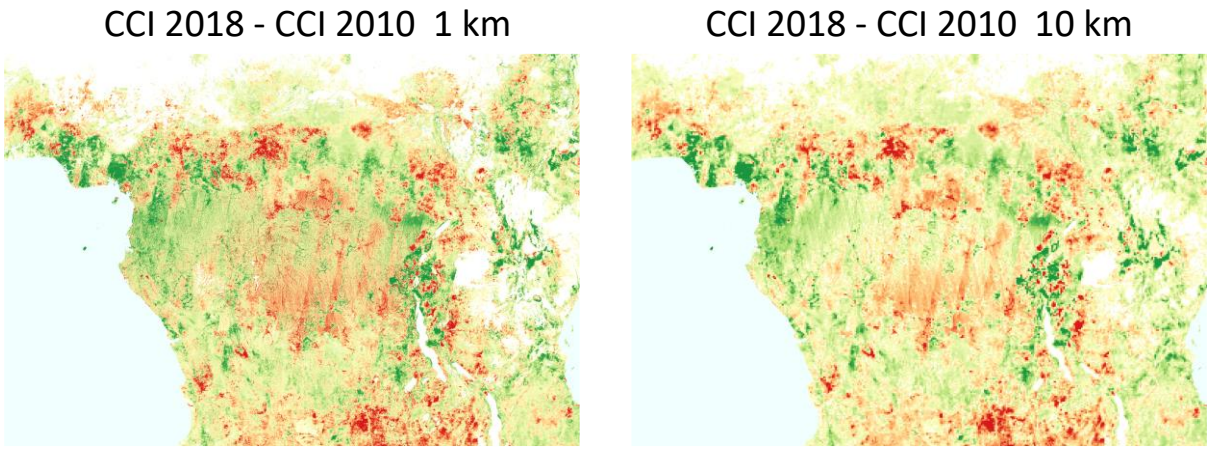

Figure 30: Maps of differences in AGB in the Congo basin, from the CCI AGB maps of 2018, and 2010, at 1 km resolution (left), and at 10 km resolution (right).

For the time being, the map of differences in AGB from the CCI maps at resolution of 1 km or < 1 km, even with the help of SMOS VOD time series for 'recalibrating' of 2010 CCI AGB map, (or recalibrating 2027/2018 CCI maps) will be difficult to interpret with respect to an increase or decrease of AGB. This is particularly the case in tropical forest, where quantitative carbon loss and gain need to be estimated.
Alternative approaches which could be considered for the AGB change estimates:

1) To generate the best possible AGB maps from L VOD at 25 km resolution , for carbon budget estimation and for use as input or verification of vegetation models (such as Dynamic Vegetation models).
2) With the condition of access to strip data (e.g. from JAXA for ALOS-2 PALSAR-2), to generate high resolution (100 m) AGB maps with reduced strip effects, e.g. for Phase 2 of the project.

3. References

Archibald, S., Scholes, R., 2007. Leaf green-up in a semi-arid African savanna-separating tree and grass responses to environmental cues. *Journal of Vegetation Science*, 18, 583–594.

Asbridge, E., Lucas, R.M., Ticehurst, C. and Bunting, P. (2016). Mangrove response to environmental change in Australia's Gulf of Carpentaria. *Ecology and Evolution*. 10.1002/ece3.2140

Bunting, P., Rosenqvist, A., Lucas, R., Rebelo, L.-M., Hilarides, L., Thomas, N., Hardy, A., Itoh, T., Shimada, M. and Finlayson, C., 2018. The Global Mangrove Watch—A New 2010 Global Baseline of Mangrove Extent. *Remote Sensing*, 10(10), 1669. http://doi.org/10.3390/rs10101669

Cartus, O., Santoro, M., Wegmüller, U., & Rommen, B. (2019). Benchmarking the retrieval of biomass in boreal forests using P-Band SAR backscatter with multi-temporal C-and L-Band observations. *Remote Sensing*, *11*(14), 1695.

Chave, J., Réjou-Méchain, M., Búrquez, A., Chidumayo, E., Colgan, M.S., Delitti, W.B., Duque, A., Eid, T., Fearnside, P.M., Goodman, R.C. and Henry, M., 2014. Improved allometric models to estimate the aboveground biomass of tropical trees. *Global Change Biology*, 20, 3177–3190.

DiMiceli, C., Carroll, M., Sohlberg, R., Kim, D. H., Kelly, M. and Townshend, J. R. G. (2015). MOD44B MODIS/Terra Vegetation Continuous Fields Yearly L3 Global 250m SIN Grid V006 [Data set]. NASA EOSDIS Land Processes DAAC.

Di Gregorio A. and Jansen, L.I.M. (2005) Land Cover Classification System Classification concepts and user manual Software version (2). In: 8 EaNRS (ed). Food and Agriculture Organization of the United Nations, Rome.

Hansen, M.C., Potapov, P.V., Moore, R., Hancher, M., Turubanova, S.A.A., Tyukavina, A., Thau, D., Stehman, S.V., Goetz, S.J., Loveland, T.R. and Kommareddy, A., 2013. High-resolution global maps of 21st-century forest cover change. *science*, *342*(6160), pp.850-853.

Labriere, N., Tao, S., Chave, J., Scipal, K., Le Toan, T., Abernethy, K., Alonso, A., Barbier, N., Bissiengou, P., Casal, T. and Davies, S.J., 2018. *In situ* reference datasets from the TropiSAR and AfriSAR campaigns in support of upcoming spaceborne biomass missions. *IEEE Journal of Selected Topics in Applied Earth Observations and Remote Sensing*, (99), pp.1-11.

Lucas, R.M., Van De Kerchove, R., Otero, V., Lagomasino, D., Fatoyinbo, L., Hamdan, O., Satyanarayana, B. and Dahdouh-Guebas, F. (2019). Structural characterisation of mangrove forests achieved through combining multiple sources of remote sensing data. Remote Sesning of Environment, 237, 111543. https://doi.org/10.1016/j.rse.2019.111543

Lucas, R.M., Otero, V., Van De Kerchove, R., Lagomasino, D., Satyanarayana, B. and Dahdouh-Guebas, F. (2020a). Automated quantification of mangrove change from multi-modal Earth

Observation data, Matang Forest Mangrove Reserve, Malaysia. LAND. https://doi.org/10.1002/ldr.3652.

Lucas, R.M., Mueller, N., Siggins, A., Owers, C., Clewley, D., Bunting, P., Kooymans, C., Tissott, B., Lewis, B., Lymburner, L. and Metternicht, G. (2020b). Land cover mapping using Digital Earth Australia. Data, 4, 143; https://doi.org/10.3390/data4040143.

Mermoz, S., Réjou-Méchain, M., Villard, L., Le Toan, T., Rossi, V. and Gourlet-Fleury, S., 2015. Decrease of L-band SAR backscatter with biomass of dense forests. *Remote Sensing of Environment*, *159*, pp.307-317.

Nilsson, M., Nordkvist, K., Jonzén, J., Lindgren, N., Axensten, P., Wallerman, J., Egberth, M., Larsson, S., Nilsson, L., Eriksson, J. and Olsson, H., 2017. A nationwide forest attribute map of Sweden predicted using airborne laser scanning data and field data from the National Forest Inventory. *Remote Sensing of Environment*, *194*, pp.447-454.

Paul, K.I., Roxburgh, S.H., Chave, J., England, J.R., Zerihun, A., Specht, A., Lewis, T., Bennett, L.T., Baker, T.G., Adams, M.A. and Huxtable, D., 2016. Testing the generality of above-ground biomass allometry across plant functional types at the continent scale. *Global change biology*, *22*(6), pp.2106-2124.

Ploton et al., 2020. A map of African humid tropical forest aboveground biomass derived from management inventories. *Scientific Data*, *7*(1), 1-13

Rejou-Mechain, M., Muller-Landau, H.C., Detto, M., Thomas, S.C., Toan, T.L., Saatchi, S.S., Barreto-Silvia, J.S., Bourg, N.A., Bunyavejchewin, S., Butt, N. and Brockelman, W.Y., 2014. Local spatial structure of forest biomass and its consequences for remote sensing of carbon stocks. *Biogeosciences Discussions*, *11*, p.5711.

Rodríguez-Fernández, N. J., Mialon, A., Mermoz, S., Bouvet, A., Richaume, P., Al Bitar, A., ... & Kerr, Y. H. (2018). An evaluation of SMOS L-band vegetation optical depth (L-VOD) data sets: high sensitivity of L-VOD to above-ground biomass in Africa. *Biogeosciences*, *15*(14), 4627-4645.

Rodríguez-Veiga, P., Quegan, S., Carreiras, J., Persson, H.J., Fransson, J.E., Hoscilo, A., Ziółkowski, D., Stereńczak, K., Lohberger, S., Stängel, M. and Berninger, A., 2019. Forest biomass retrieval approaches from earth observation in different biomes. *International Journal of* Applied Earth Observation and Geoinformation, 77, pp.53-68.

Ryan, C.M., Williams, M., Grace, J., 2011. Above-and Belowground Carbon Stocks in a Miombo Woodland Landscape of Mozambique. *Biotropica*, 1–10.

Simard, M., Pinto, N., Fisher, J.B. and Baccini, A., 2011. Mapping forest canopy height globally with spaceborne lidar. *Journal of Geophysical Research: Biogeosciences*, *116*(G4).

Simard, M., Fatoyinbo, L., Smetanka, C., Rivera-Monroy, V. H., Castañeda-Moya, E., Thomas, N., & Van der Stocken, T., 2019. Mangrove canopy height globally related to precipitation, temperature and cyclone frequency. *Nature Geoscience*, 12(1), 40–45.

Villard, L. and Le Toan, T., 2015. Relating P-Band SAR Intensity to Biomass for Tropical Dense Forests in Hilly Terrain: *IEEE Journal of Selected Topics in Applied Earth Observations and*

Remote Sensing, *8*(1), pp.214-223.

Watanabe, M., Koyama, C. N., Hayashi, M., Nagatani, I. and Shimada, M. (2018). Early-Stage Deforestation Detection in the Tropics With L-band SAR, *IEEE Journal of Selected Topics in Applied Earth Observations and Remote Sensing*, 11, 2127-2133doi: 10.1109/JSTARS.2018.2810857.

Xu, L., Saatchi, S.S., Shapiro, A., Meyer, V., Ferraz, A., Yang, Y., Bastin, J.F., Banks, N., Boeckx, P., Verbeeck, H. and Lewis, S.L., 2017. Spatial distribution of carbon stored in forests of the Democratic Republic of Congo. *Scientific reports*, *7*(1), p.15030.